

# Carbon Monoxide Climatology derived from the Trajectory Mapping of Global MOZAIC-IAGOS Data

M. [K. Osman](#)<sup>1,\*</sup>, D.W. Tarasick<sup>1</sup>, J. Liu<sup>2</sup>, O. Moeini<sup>1</sup>, V. Thouret<sup>3</sup>, V. E. Fioletov<sup>1</sup>, M. Parrington<sup>4</sup>, P. Nédélec<sup>3</sup>

<sup>1</sup>Environment Canada, 4905 Dufferin Street, Downsview, ON, M3H 5T4 Canada

<sup>2</sup>Department of Geography and Program in Planning, University of Toronto, 100 St. George Street, Toronto, Ontario, M5S 3G3, Canada

<sup>3</sup>Laboratoire d'Aérodynamique, UMR5560, CNRS and Université de Toulouse, Toulouse, France

<sup>4</sup>European Centre for Medium-Range Weather Forecasts, Shinfield Park, Reading, RG2 9AX, UK

[\\*now at: Cooperative Institute for Mesoscale Meteorological Studies, The University of Oklahoma, and NOAA/National Severe Storms Laboratory, Norman, Oklahoma, USA](#)

## Abstract

A three-dimensional gridded climatology of carbon monoxide (CO) has been developed by trajectory mapping of global MOZAIC-IAGOS in situ measurements from commercial aircraft data. CO measurements made during aircraft ascent and descent, comprising nearly 41,200 profiles at 148 airports worldwide from December 2001 to December 2012 are used. Forward and backward trajectories are calculated from meteorological reanalysis data in order to map the CO measurements to other locations, and so to fill in the spatial domain. This domain-filling technique employs 15,800,000 calculated trajectories to map otherwise sparse MOZAIC-IAGOS data into a quasi-global field. The resulting trajectory-mapped CO dataset is archived monthly from 2001-2012 on a grid of 5° longitude×5° latitude×1 km altitude, from the surface to 14 km altitude.

The mapping product has been carefully evaluated, [first](#) by comparing maps constructed using only forward trajectories and using only backward trajectories. The two methods show similar global CO distribution patterns. The magnitude of their differences is most commonly 10% or less, and found to be less than 30% for almost all cases. The ~~trajectory-mapped CO dataset~~[method](#) has also been validated by ~~comparison~~[comparing](#) profiles for individual airports with those produced by the mapping method when data from that site are excluded. While there are larger differences below 2 km, the two methods agree very well between 2 and 10 km with the magnitude of biases within 20%. [Finally, the mapping product is compared with global MOZAIC-IAGOS cruise-level data, which were not included in the trajectory-mapped dataset, and with independent data from the NOAA aircraft flask sampling program.](#)

Maps are also compared with Version 6 data from the Measurements Of Pollution In The Troposphere (MOPITT) satellite instrument. Both data sets clearly show major regional CO sources such as biomass burning in central and southern Africa and anthropogenic emissions in eastern China. While the maps show similar features and patterns, and agreement is good relative biases are small in the lowermost troposphere, the MOPITT CO profile shows negative biases we find differences of ~20% in CO volume mixing ratios between 500 hPa and 300 hPa. These upper troposphere biases are not related to the mapping procedure, as almost identical differences are found with the original in situ MOZAIC-IAGOS data. The total CO trajectory-mapped MOZAIC-IAGOS ~~climatology~~ column agrees with ~~is also higher than~~ the MOPITT CO total column, by within  $\pm 5$ –16%, which is consistent with previous reports.

~~The maps clearly show major regional CO sources such as biomass burning in the central and southern Africa and anthropogenic emissions in eastern China.~~ The dataset shows the seasonal CO cycle over different latitude bands and altitude ranges ~~that are representative of the regions~~ as well as long-term trends over different latitude bands. We observe a decline in CO over the northern hemisphere extratropics and the tropics consistent with that reported by previous studies using other data sources.

~~Similar maps have been made using the concurrent  $O_3$  measurements by MOZAIC-IAGOS, as the global variation of  $O_3$ -CO correlations can be a useful tool for the evaluation of ozone sources and transport in chemical transport models.~~ We anticipate ~~use~~ of the trajectory-mapped MOZAIC-IAGOS CO dataset as an a priori climatology for satellite retrieval, and for air quality model validation and initialization.

## 1 Introduction

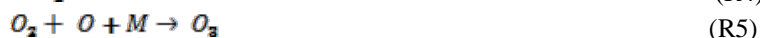
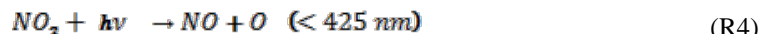
Atmospheric carbon monoxide (CO) is an important global air pollutant and trace gas. Due to its relatively long lifetime of 1-4 months (Hubler et al., 1992; Law and Pyle, 1993), it is an ideal tracer for long range atmospheric transport (Logan et al., 1981; Lelieveld et al., 2001; Shindell et al., 2006). Moreover, in the tropics, it is an important tracer of upward transport during convective events (e.g., Pommrich et al., 2014). Consequently, it has been employed to facilitate interpretations of chemical measurements (Jaffe et al., 1996; Parrish et al., 1991, 1998; Wang et al., 1996, 1997) and in validating chemical transport models (Carmichael et al., 2003; Liu et al., 2003; Tan et al., 2004; Wang et al., 2004). The main sources of atmospheric CO are relatively well understood (Galanter et al., 2000; Granier et al., 2011; Holloway et al., 2000); however, the magnitude of individual sources and their seasonal variability, especially of biomass burning, are not well quantified. Stein et al. (2014) also reported that models are also generally biased low due to either an underestimation of CO sources or an overestimation of its sinks. There are differences in the emission densities of anthropogenic and natural sources, despite the fact that the anthropogenic and natural sources are of similar magnitude on a global scale (Granier et al., 2011; Logan et al., 1981). The anthropogenic sources are primarily associated with large industrial centers or major biomass burning regions while the natural sources, such as oxidation

of methane (CH<sub>4</sub>) and non-methane hydrocarbons (NMHCs) are much more diffuse. This makes CO a good atmospheric tracer gas for anthropogenic emissions as its lifetime allows it to be used as an indicator of how large-scale atmospheric transport redistributes pollutants on a global scale.

CO plays a vital role in the chemistry of the atmosphere. This significance mainly comes from the influence of CO on the concentrations and distributions of the atmospheric oxidants, ozone (O<sub>3</sub>), the hydroperoxy (HO<sub>2</sub>) and hydroxyl radicals (OH) (e.g. Novelli et al., 1994, 1998). Reaction (R1) between CO and OH represents 90-95% of the CO sink (Logan et al., 1981), and about 75% of the removal of OH (Thompson, 1992) in the troposphere:



In areas with sufficient NO<sub>x</sub> (=NO + NO<sub>2</sub>), HO<sub>2</sub> formed in reaction (R2) leads to photochemical reactions (R3)-(R5) which bring about net O<sub>3</sub> production. In urban areas and regions of biomass burning, large amounts of these O<sub>3</sub> precursors will be produced, and O<sub>3</sub> can be formed in, and downwind of, the source region (Crutzen, 1973; Fishman and Seiler, 1983):



O<sub>3</sub> is associated with respiratory problems and decreased crop yields (e.g., McKee, 1993; Chameides et al., 1994). Since CO and OH are principal reaction partners, CO concentrations in the atmosphere have important climatological implications. OH is also responsible for the removal of greenhouse gases such as CH<sub>4</sub>, and other volatile organic compounds in the atmosphere. Via these interactions with OH, O<sub>3</sub> and CH<sub>4</sub>, CO has an indirect radiative forcing of about 0.25 W m<sup>-2</sup> (IPCC AR5).

Global atmospheric chemistry models require accurate CO concentrations on a global scale in order to define spatial and temporal variations of atmospheric oxidants and CO. For this reason measurements of CO are made by different kinds of remote sensing and in situ instruments, in ground-based networks, aircraft programmes and from space (Novelli et al., 1994, 1998; Rinsland and Levine, 1985; Zander et al., 1989; Brook et al., 2014; Reichle et al., 1990; 1999; Worden et al., 2013; Petzold et al., 2015). [Long range atmospheric transport redistributes CO widely due to its relatively long lifetime. Typical tropospheric background CO levels range between 50 and 120 ppbv \(WHO, 2000\). Background CO levels are found in all regions of the troposphere, where mixing ratios between 45 and 250 ppbv have been reported \(Novelli et al., 1994\). Extreme m](#)Mixing ratios much higher than 250 ppb have been observed in the upper troposphere over Asia (Nédélec et al., 2005) or over the Pacific (Clark et al., 2015) in [biomass burning plumes of boreal biomass burning. CO values as high as 1800 ppbv have been reported](#)

~~over Beijing (Zbinden, et al., 2013). The largest values in the lower troposphere have been observed over Beijing (Zbinden et al., 2013).~~

Early studies of ground-based observations showed increasing trends in global CO before 1980 (Khalil and Rasmussen, 1988; Rinsland and Levine, 1985; Zander et al., 1989), followed by a modest decline in the 1990s (Novelli et al. 1994; 2003; Khalil and Rasmussen, 1994). More recently satellite observations have shown that the decline has continued: Worden et al. (2013) report a global trend from 2000-2011 of ~10% per decade on column CO in the northern hemisphere. Petetin et al. (2015) show a similar decrease of about 2 ppb per year over Frankfurt throughout the troposphere from 2002 to 2012. The decrease is at least partly due to a decrease in global anthropogenic CO emissions (Granier et al., 2011).

In-service Aircraft for a Global Observing System (IAGOS), and its predecessor Measurement of Ozone and water vapor by Airbus in-service airCRAFT (MOZAIC), have been making automatic and regular measurements of O<sub>3</sub>, water vapour and standard meteorological parameters onboard long-range commercial Airbus A340 aircraft since August 1994 (Marengo et al., 1998, Petzold et al., 2015). Measurements of CO (Nédélec et al., 2003) and NOy (~~the sum of NOx plus its atmospheric oxidation products~~) (Volz-Thomas et al., 2005) were added in late 2001. The MOZAIC database currently contains data from more than ~~71,900 vertical profiles of O<sub>3</sub> and~~ 41,200 vertical profiles of CO, measured during takeoff and landing from 148 airports around the world. MOZAIC measurements show the general features of the atmospheric CO distribution (Zbinden et al., 2013; Petzold et al., 2015 and references therein), capturing major regional features (e.g., strong CO emissions from biomass burning or anthropogenic sources).

The objective of this paper is to present a three-dimensional (i.e., latitude, longitude, altitude) gridded climatology of carbon monoxide that has been developed by trajectory mapping of global MOZAIC-IAGOS CO data from 2001-2012. We employ a domain-filling technique, using approximately 15,800,000 calculated trajectories to map otherwise sparse MOZAIC-IAGOS CO data into a global field.

This is a technique that has been used successfully with tropospheric and stratospheric ozonesonde data (G. Liu et al., 2013; J. Liu et al., 2013). Stohl et al. (2001) used trajectory statistics to extend one year of MOZAIC O<sub>3</sub> measurements into a 4-season O<sub>3</sub> climatology at 10° longitude by 6° latitude and three vertical heights. Tarasick et al. (2010) developed high resolution (1°×1°×1 km in latitude, longitude, and altitude) tropospheric O<sub>3</sub> fields for North America from ozonesonde data from the INTEX (Intercontinental Transport Experiment) and ARCTAS (Arctic Research of the Composition of the Troposphere from Aircraft and Satellites) campaigns, and this was extended to global tropospheric ozonesonde data by G. Liu et al. (2013). It is possible to apply this technique to CO because the lifetime of CO in the troposphere, as noted above, is generally of the order of weeks or months. This physically-based ~~interpolation~~ method, using the reanalysis meteorological data from the National Centers for Environmental Prediction/National Center for Atmospheric Research (NCEP/NCAR) (Kalnay et al., 1996) ~~to, in~~

effect, interpolate data based on knowledge of atmospheric transport, offers obvious advantages over typical statistical interpolation methods. Indeed, it is expected to improve global models and satellite data validation and it can also be used as a priori for satellite data retrieval.

Major regional features of the global CO distribution are clearly evident in the global maps thus produced, especially regions of intense biomass burning or anthropogenic pollution. The 3D global trajectory mapped CO climatology facilitates visualization and comparison of different years, decades, and seasons, and offers insight into the global variation of CO. Moreover, it will be useful for climate and air quality model initialization and validation, and can be used as an a priori climatology for satellite data retrievals. Comparison with similar maps made using the concurrent  $O_3$  measurements by MOZAIC-IAGOS allow us to examine the global variation of  $O_3$ -CO correlations, which convey information about the source distribution of CO.  $O_3$ -CO correlations are also of great interest around the tropopause region since such correlations provide information on mixing processes (e.g., Hoor et al., 2004; Pan et al., 2006; Vogel et al., 2011) besides of the source regions. This paper is organized in the following order. Following discussion of the MOZAIC-IAGOS and MOPITT instruments in Sect. 2.1 and 2.2, respectively, we describe trajectory mapping calculation via HYSPLIT model in Sect. 2.3. The transformation of MOZAIC-IAGOS data by applying the MOPITT a priori profile and averaging kernels is presented in Sect. 2.4. The validation of the trajectory mapped dataset against MOZAIC-IAGOS in situ data will be presented in Sect. 3. The same section assesses the differences between the CO mapping produced using only backward and only forward trajectories, and also compares with in situ global CO data at cruise altitudes between 8 and 12 km. Subsequently, the comparison of the trajectory mapped MOZAIC-IAGOS CO with MOPITT CO retrievals is presented in Sect. 4. Section 5 discusses the results obtained from the global 3D trajectory-mapped climatology data. After pointing out the potential applications of the trajectory-mapped MOZAIC-IAGOS CO climatology (i.e.,  $O_3$ -CO relationship and global variation and trends of CO) and data coverage and the associated standard errors in Sect. 6, we make concluding remarks about the results we obtain from this study in Sect. 7.

## 2 Measurements of CO

### 2.1 MOZAIC-IAGOS

CO measurements were made by an improved version of a commercial Model 48CTL CO Analyzer from Thermo Environmental Instruments employing the Gas Filter Correlation technique. The Model 48CTL is based on the principle that CO absorbs infrared radiation at a wavelength of 4.67 microns. For 30 s integration time (the response time of the instrument) the precision achieved is 5 ppb (noise) or 5% (calibration) CO, with minimum detection limit of 10 ppb. The analyzer samples at a horizontal resolution of about 7 km (since the maximum cruise speed of the Airbus A340 aircraft is nearly 250 m/s) and the vertical resolution during ascents and descents is nearly 300 m. Nedelec et al. (2003 for MOZAIC, 2015 for IAGOS) give detailed

descriptions of the CO analyzer, measurement technique, instrument validation and quality testing.

The airports visited by aircraft equipped with MOZAIC-IAGOS instrumentation are shown in Fig. 1. Further details are available at <http://www.iagos.fr>.

**Fig. 1.** Airports ~~stations~~ visited by MOZAIC-IAGOS aircraft from 2001-2012. The color bar indicates the number of profiles available from each airport. The squares show the locations of the selected airports used for the validation in this study.

The sampled data from these airports are unevenly distributed ~~both~~ spatially, and also temporally because the frequency of visits to airports by aircraft that take part in MOZAIC-IAGOS varies considerably depending on commercial airlines' operational constraints. ~~This-Thus means that at airports such as~~ Frankfurt, Germany we find ~~as many as~~ 12,324 CO profiles while from Dammam, Saudi Arabia we have only 2 ~~CO profiles~~ during the period 2001-2012. The trajectory-mapping method is valuable for filling the sparse and variable spatial domain.

## 2.2 MOPITT

MOPITT is a nadir-viewing gas correlation radiometer which provides global atmospheric profiles of CO volume mixing ratio (VMR) and CO total column values using near-infrared radiation at 2.3  $\mu\text{m}$  and thermal-infrared radiation at 4.7  $\mu\text{m}$  ([Drummond and Mand, 1996](#)). CO columns and profiles are retrieved from the IR emission channels (4.6  $\mu\text{m}$ ) for all cloud-free scenes. The MOPITT measurement technique relies on a temperature gradient within the atmosphere ~~thermal contrast between the Earth's surface and atmosphere~~, leading to a retrieval dependence on surface temperature, and little sensitivity to CO in the boundary layer. The retrieval uses a priori profiles that vary geographically and temporally. MOPITT-derived CO VMR profiles reflect the vertical sensitivity of the measurement as defined by the retrieval averaging kernel (e.g. Fig. [23](#)) and a priori profile. In this study, we have used Level 3, Version 6 monthly CO mixing ratio profile data, reported on 10 pressure levels, as well as CO total column. Nighttime CO observations of MOPITT have not been validated and appear subject to larger bias (Heald et al., 2004). Hence, we use the daytime data for comparison. MOPITT data are publicly available at the NASA Langley Research Center Atmospheric Science Data Center: [https://eosweb.larc.nasa.gov/project/mopitt/mopitt\\_table](https://eosweb.larc.nasa.gov/project/mopitt/mopitt_table).

MOPITT was launched in 1999 into sun-synchronous polar orbit with a 1030 local time (LT) northward or southward ~~local~~ equator cross-over time. The instrument field of view is 22x22  $\text{km}^2$ . Cross-track scanning with a 612 km swath provides near complete coverage of the surface of the Earth approximately every 3 days. MOPITT retrievals have gone through intensive

validation against in situ measurements from aircraft on a regular basis since the start of the mission (Worden et al., 2010; Deeter et al., 2012, 2013, 2014; Emmons et al., 2004, 2007, 2009; Jacob et al., 2003). MOPITT CO retrievals have also been validated by comparing to ground-based and TES satellite measurements (Jacob et al., 2003 and [Lou-Luo et al., 2007](#)). [Deeter et al. \(2014\)](#) employ the MOPITT L3 V6 product and showed biases to vary from -5.2% at 400 hPa to 8.9% at the surface. ~~However, most of previous studies focused on the earlier versions of the MOPITT product. In the lower troposphere a mean positive bias of 6-8% against in situ validation profiles has been reported, and a mean bias and standard deviation for the retrieved CO column of  $5 \pm 11\%$  and  $0.5 \pm 12.1\%$  for periods, respectively, March 2000–May 2001 and August 2001–December 2002 (Emmons et al., 2004). Jacob et al. (2003) reported the CO bias to be  $6 \pm 2\%$ , where as Emmons et al. (2007) found approximately  $7 \pm 8\%$  bias for summer 2004 measurements. Deeter et al. (2013) also show a total column retrieval bias of about  $0.08 \times 10^{18}$  molecules/cm<sup>2</sup> ( $\sim 4\%$ ) against in situ profiles. Furthermore, Deeter et al. (2012) reported a positive bias of surface-level CO concentrations on the order of a few percent against in situ profiles.~~

### 2.3 Trajectory calculation and global CO mapping via HYSPLIT

For each CO profile of the MOZAIC-IAGOS data set presented here, the mean CO VMR was calculated for 1-km intervals from sea level up to 12 km (the maximum altitude of the aircraft). Cruise data were not used. The HYSPLIT (Hybrid Single-Particle Lagrangian Integrated Trajectory) model version 4.9 (Draxler and Hess, 1998, Draxler, 1999) was employed to calculate trajectories for each level of each profile. ~~We used~~ [The exact location of the aircraft was used to start the trajectories.](#) HYSPLIT, publicly accessible at (<http://ready.arl.noaa.gov/HYSPLIT.php>), uses the reanalysis meteorological wind fields from the National Centers for Environmental Prediction/National Center for Atmospheric Research (NCEP/NCAR) (Kalnay et al., 1996) as an input to describe the transport of CO in the atmosphere. The reanalysis data are ~~readily~~ available from 1948 until the present. Both forward and backward trajectories for 4 days at 6-hour intervals (32 positions for each level) were calculated for 41,200 CO profiles, and the mean CO mixing ratios from each level (i.e., tropospheric and lower stratospheric air masses) of each profile were assigned to the corresponding trajectory positions along the forward and backward paths. Trajectories only move upward and downward with the meteorological vertical velocity fields since the HYSPLIT kinematic trajectory model employs vertical motions supplied with the NCEP reanalysis meteorological data set. Numerous studies show that the choice of vertical wind velocity has significant impact on the transport of tracers (e.g., Schoeberl et al. 2003; Ploeger et al., 2010, 2012). Kinematic models show excessive dispersion for tracers with strong gradients (e.g., O<sub>3</sub> in the vicinity of the tropopause), particularly for trajectories of 7 days or more. ~~We limit~~ [Here trajectories were limited](#) to a maximum ~~offer~~ 4 days in length. Moreover, unlike O<sub>3</sub>, CO does not have [a](#) strong vertical gradient in the upper troposphere. Trajectories that reach the ~~bottom boundary (i.e., ground)~~ continue at the surface where ~~the trajectory robustness grows to be is~~



more uncertain. Trajectories that reach the top height of the model (20,000 m above sea level) will terminate. Although HYSPLIT is capable of generating a trajectory every hour (i.e., 24 trajectories per day), the ~~average available~~ typical maximum frequency of CO measurements (~~if the MOZAIC IAGOS aircraft visits the airports~~) is around 2 profiles per day (with the exception of Frankfurt where we can get up to 6 profiles per day). In this version, trajectory mapped ~~MOZAIC IAGOS CO climatology, we did not~~ attempt was made to exclude identify major individual anthropogenic CO sources; however, the climatology could in principle be refined by excluding backtrajectories from ~~sources~~ identified via emission inventories. We note, however, that if major anthropogenic sources were a significant source of error, we would see differences between the CO mapping produced using only backward and only forward trajectories (see Sect. 3.1).

This mapping implicitly assumes that CO chemistry may be neglected over a timescale of 4 days. Except near major ~~anthropogenic~~ sources, this assumption should be valid, as the lifetime of CO is much longer. However, trajectories have significant errors over such timescales. Stohl (1998) in a comprehensive review, quotes typical errors of about 100-200 km/day in the troposphere. This can be combined with an estimate of the correlation length in the troposphere to yield an estimate for the information value of a mapped measurement. Liu et al. (2009) find that O<sub>3</sub> measurements in the troposphere correlate with an exponential dependence of approximately  $e^{-(r/R)^{1.5}}$ , ~~where with  $r$  shown in Eq. (1)) is distance and  $R$  is a correlation length of 500-1000 km in the troposphere, and 1000-2000 km in the stratosphere. The means that the horizontal distance for the correlation coefficient to decrease by a factor of  $e$  is 500-1000 km in the troposphere and 1000-2000 km in the stratosphere.~~ As the CO lifetime is even longer than the ozone lifetime, the correlation length for CO should be at least as large. Therefore, the trajectory-mapped data were binned at intervals of 5° latitude and 5° longitude, at every 1-km altitude, and averaged with a weighting,  $w$ , assigned according to the formula:

$$w = e^{-(150t/R)^{1.5}} \quad (1)$$

where  $R$  is the correlation length (taken as 700 km and 1500 km in the troposphere and 1500 km and in the stratosphere, respectively), and  $t$  is the age of the trajectory in days.

The trajectory mapping greatly spreads out the in situ CO information along the trajectory paths, increasing the spatial domain to include much of the globe. Two different vertical coordinate systems were utilized for the binning, and hence the maps were generated for elevations above sea level and above ground level. Data are available publicly at [ftp://es-ee.tor.ec.gc.ca/pub/ftpdt/MOZAIC\\_output\\_CO/ftp://es-ee.tor.ec.gc.ca/pub/ftpdt/](ftp://es-ee.tor.ec.gc.ca/pub/ftpdt/MOZAIC_output_CO/ftp://es-ee.tor.ec.gc.ca/pub/ftpdt/). In this work, we present global CO maps generated for elevations above sea level. Global maps of monthly, annual, seasonal and decadal means are presented, for each altitude, from 2001-2012.

## 2.4 Distribution of data and uncertainties associated with trajectory mapping

Field Code Changed



Figure 4A2 shows typical standard errors of the mapping product and the number of samples per grid cell, for typical monthly, annual and decadal maps at 4.5 km altitude above sea level. Similar figures for other levels are included with the climatology on the FTP site. As can be seen, the largest number of samples per grid cell and the lowest standard errors are found over North America and Europe as there are more frequent MOZAIC-IAGOS aircraft flights in this region. Higher standard errors are found at NH high latitudes and much of the SH, where airports visits by MOZAIC-IAGOS-equipped aircraft are much fewer. The standard error is computed using all data points found inside a grid cell. This is probably biased low, since some grid cells may contain more than one value from a particular trajectory. This bias is likely not more than a factor of 2, based on typical trajectory lengths. These maps present a visual interpretation that distinguishes regions where the CO climatology is 'statistically robust' (for example, North America and Europe) from those regions where the uncertainty is larger. The average number of samples is approximately 20, 90, and 140 per grid cell for the monthly, annual and decadal maps, and this number does not vary greatly among layers. The average standard error is generally between 3 and 4% of the mean at 4.5 km for all three averaging periods. The monthly mean shows the highest error and the lowest number of samples per grid cell.

Fig. 4A2 The standard error of the mean (left panels) and number of samples (right panels) for monthly (July 2012), annual (2005), seasonal (DJF 2001-2012) means at 4.5 km altitude above sea level. The month and year shown are chosen as typical; other months and years show similar patterns. The data are binned on a  $5^\circ \times 5^\circ$  latitude and longitude grid.

## 2.4.5 MOZAIC-IAGOS Comparison with MOPITT

When comparing the MOPITT retrievals with in situ data, it is necessary to take into account the sensitivity of the retrievals to the true profiles. The method used by MOPITT to retrieve tropospheric CO profiles follows that of Rodgers (2000). In order to perform the most meaningful and accurate comparison, the in situ data to be compared must be transformed using the averaging kernel matrix,  $A$ , and a priori profile,  $x_a$ , as shown by Eq. (2). A "retrieved" comparison profile,  $x_{ret}$ , is calculated by using the in situ profile,  $x$ , as the "true" profile in Eq. (2) which is interpolated to the lower resolution of MOPITT. As described by Emmons et al. (2004), the in situ profile ( $x$ ) is transformed with averaging kernel matrix ( $A$ ) and the a priori CO profile ( $x_a$ ) to get a profile ( $x_{ret}$ ), the appropriate quantity to compare with the MOPITT retrievals:

$$x_{ret} = x_a + A(x - x_a) + \varepsilon = Ax + (I - A)x_a + \varepsilon \quad (2)$$

where  $I$  is the identity matrix and  $\varepsilon$  is the retrieval error due to random errors in the measurement and systematic errors in the forward model (e.g., the error in the atmospheric temperature retrieval).  $x_{ret}$ ,  $x$ , and  $x_a$  are expressed in terms of the logarithm of the VMR.

The averaging kernels provide the relative weighting between the true and a priori profiles and reflect the sensitivity of the retrieval to the measurement (Worden et al., 2013). They are very sensitive to the surface temperature and will be different for each point on the globe. The matrix  $A$  describes the sensitivity of the retrieved CO log(VMR) profile to perturbations applied at each level of the “true” log(VMR) profile. The quantity  $x_{ret}$ , the transformed in situ profile, represents the result of applying a linear transformation to the in-situ profile in the same way that the remote sensing retrieval process is believed to transform the true profile. Thus,  $x_{ret}$  can be directly compared against the MOPITT retrieved CO profile in a manner that is not affected by varying vertical resolution or a priori dependence.  $x_{ret}$ ,  $x$ , and  $x_a$  are expressed in terms of the natural/common logarithm of the volume mixing ratio (VMR), i.e.,  $\log_e(VMR)/\log_{10}(VMR)$ .

The vertical resolution of the retrieved profile is described by the shapes of the averaging kernels. Figure 2-3 shows that the kernels are broad except at pressure levels between 400-300 hPa and exhibit a large degree of overlap. The overlap of the averaging kernels peaking in the boundary layer and those at the top of the atmosphere indicates a significant correlation for the retrieved values at these levels. Typical full-width at half maximum (FWHM) of these curves is approximately 5-8 km. The retrieved CO values at these levels both top and bottom are also influenced by CO at mid levels, and by the a priori CO profile at all pressure levels. The averaging kernels also describe the relative contributions, to the CO VMR retrieved at a given level, of the true and a priori (via I - A) CO profiles at all pressure levels (Eq. (2)). Where the area under the averaging kernel is smaller, the a priori information in the retrieved CO profile is relatively larger. MOPITT CO averaging kernels exhibit variability from month to month, season to season as well as nighttime to daytime, depending on the atmospheric temperature profile, surface pressure and the CO profile itself.

The vertical coordinate of the MOZAIC-IAGOS climatology profile is kilometers above sea level, while the MOPITT a priori profile and averaging kernels are on pressure levels in hPa. Therefore, before applying the MOPITT averaging kernels the climatology data were interpolated using NCEP global pressure profiles that vary as a function of time (month) and latitude, to the 10 vertical pressure grid levels (1000, 900, 800, 700, 600, 500, 400, 300, 200, and 100 hPa) used by MOPITT. The interpolated profile was then convolved with the a priori profile and the averaging kernels following Eq. (2) (Emmons et al., 2004). For the atmospheric residual above the maximum MOZAIC-IAGOS profile altitude, the MOPITT a priori profiles were used.

In order to compare with these transformed CO profiles, the MOPITT CO profiles, averaging kernels, and a priori profiles were mapped down from the original horizontal resolution of  $1^\circ \times 1^\circ$  in latitude and longitude to a reduced  $5^\circ \times 5^\circ$  grid. The mapping was linear in log pressure and volume mixing ratio of CO. An example of comparisons of trajectory-mapped MOZAIC-IAGOS CO profiles with an individual (reduced)  $5^\circ \times 5^\circ$  MOPITT CO profiles is shown in Fig. 2-3. The original trajectory mapped MOZAIC-IAGOS CO profile, the a priori profile, and the transformed trajectory mapped MOZAIC-IAGOS CO profile are shown along with the MOPITT

~~retrieved CO profile.~~ The application of the averaging kernels to the MOZAIC-IAGOS CO profile results in ~~significant a~~ vertical transformation, which can shift mixing ratios significantly at some levels. The averaging kernel, for example, identified as "1000" (i.e., surface) shows how changes to the true CO mixing ratio at all ten retrieval levels would each contribute to a change in the retrieved value at the surface at 1000 mbar. The original trajectory-mapped MOZAIC-IAGOS climatology profile is quite different from the transformed climatology profile and ~~as seen from the same figure~~ the departures of the transformed CO mixing ratio from the true mixing ratios can be as large as 60 ppb at some pressure levels.

CO total column amounts are retrieved from the MOPITT observations in addition to the profile retrievals. The retrieved CO total column  $c_{ret}$  (a scalar) is related to the retrieved profile  $x_{ret}$  (a vector) through the linear relation

$$c_{ret} = t^T x_{ret} \quad (3)$$

where T indicates the transpose operation and t is the total column vectors. The CO total column averaging kernel can be calculated from the profile averaging kernels by

$$a = t^T A \quad (4)$$

The column operator simply converts the mixing ratio for each retrieval level to a partial column amount. Using the hydrostatic relation, the operator  $t$  is expressed as

$$t = 2.120 \cdot 10^{13} \Delta p \quad (5)$$

Equation (5) is expressed in molecules/cm<sup>2</sup>/ppbv and  $\Delta p$  is the vector of the thicknesses of the retrieval pressure levels (in hPa).

**Fig. 23.** Examples of comparisons of monthly means of the trajectory-mapped MOZAIC-IAGOS CO profiles, with the corresponding MOPITT's averaging kernels, a priori and retrievals. The left panels of each subplot show the original trajectory-mapped MOZAIC-IAGOS climatology profile (green, i.e. unsmoothed ~~in the caption~~), the a priori profile ~~(black)~~, the transformed trajectory-mapped MOZAIC-IAGOS climatology profile (red, i.e. smoothed ~~in the caption~~), and the MOPITT retrieved CO profile ~~(blue)~~. The right panels ~~of each subplot~~ shows the mean averaging kernels, for different pressure levels, obtained by averaging all daytime averaging kernels in the 5°x5° latitude-longitude box centered on the coordinates indicated.

~~The different colors of the averaging kernel curves indicate the different pressure levels.~~

### 3 Validation

Validation of the trajectory-mapped MOZAIC-IAGOS CO dataset product has been performed by Eq. (1) comparing maps constructed using only forward trajectories against those constructed using only backward trajectories; and Eq. (2) comparing profiles for individual airports against those produced by the mapping method when data from that site are excluded; (3) comparing with global MOZAIC-IAGOS cruise-level data, which were not included in the trajectory-mapped dataset, and (4) comparing with independent data from the NOAA aircraft flask sampling program. The airport stations that have been selected in this validation study represent tropical and northern hemisphere midlatitude locations that are subject to different meteorological and CO source conditions.

### 3.1 Comparison of trajectory-mapped MOZAIC-IAGOS CO profiles

As a first step in validation of the trajectory-mapped climatology, Figs. 3-4 and S1 (in the Supplement) assess the differences between the CO mapping produced using only backward and only forward trajectories for different seasons using the 7.5 km level as an example. If chemistry (i.e. local sources or sinks) were a significant source of error then one would expect to see differences between these maps. In fact, the CO distribution patterns are very similar (Fig. 34). Differences are most commonly 10% or less, and found to be less than 30% for almost all cases. They are typically less than 10% at northern mid-latitudes and less than 20% in the tropics between  $\pm 30^\circ$  latitude, except in the Pacific and Atlantic oceans where they can be as large as 30%. As Fig. S1 illustrates, differences (Fig. S1) also show no distinct pattern, except for some clustering in areas where the trajectories are longest, and therefore least reliable. As differences between the two distributions are comparable with the uncertainties of the mean value estimates and not systematic, it is reasonable to combine forward and backward mapped values to produce an averaged CO map.

**Fig. 34.** Examples of the global distribution, 2001-2012, of trajectory-mapped MOZAIC-IAGOS CO (ppbv) produced using only backward (right panels) and only forward (left panels) trajectories at 7.5 km a.s.l. The panels correspond to different seasons: (a, b) December-February, (c, d) March-May, (e, f) June-August and (g, h) September-November 2001-2012.

### 3.2 Comparison between trajectory-mapped and in situ profiles

A good test of an interpolation model is to examine how it performs in areas where no data are available. Figure 4-5 compares the trajectory-mapped climatology profiles at three airport sites (Frankfurt, Germany; Houston, USA; and Tokyo, Japan) with the average of the MOZAIC-IAGOS data from each of these sites for May of 2001-2012. However, since the sampling frequency varies from airport to airport, Houston and Tokyo are not as well sampled as Frankfurt

throughout the period (Figure 1). The climatology profiles for each location were produced by excluding data from that location, but using all other MOZAIC-IAGOS data.

Generally, the profiles from the two methods agree very well and the agreement is especially good in the free troposphere, at altitudes between 2 and 10 km. Referring to the bottom panels of Fig. 45, the magnitude of the differences for most altitudes is well under 20%.

**Fig. 45.** Comparisons of trajectory-mapped MOZAIC-IAGOS CO climatology and MOZAIC-IAGOS profiles at Frankfurt, Germany (left panels), Houston, TX (middle panels), Tokyo, Japan (right panels) three sites. The top left, middle and right panels show MOZAIC-IAGOS CO climatology profiles (black) and the corresponding MOZAIC-IAGOS in situ profiles (red) of Frankfurt (Germany), Houston (TX, USA) and Tokyo (Japan) respectively for May 2001–2012. The climatology profiles for each location were produced by excluding data from that location, but using all other MOZAIC-IAGOS data. The horizontal error bar half-length is twice the standard error of the mean (equivalent to 95% confidence limits on the averages when the number of data points is large). Bottom left, middle and right panels indicate the relative difference  $[2(Clim - MOZAIC)/(Clim + MOZAIC)]$ , expressed in %, between the trajectory mapped MOZAIC-IAGOS climatology and MOZAIC-IAGOS in situ profiles from Frankfurt (Germany), Houston (USA) and Tokyo (Japan) respectively for May 2001–2012. The actual MOZAIC-IAGOS profiles are labeled as MOZAIC, while the profiles from trajectories without input from the airport station being tested are labeled as Climatology.

In Fig. 5–6 we extend the shows seasonally-averaged comparisons shown in Fig. 4 for other seasons as well as for another airports that represent different meteorological and source conditions differences, using this method, for a number of airports with different characteristics. The airport stations that have been selected in this validation study represent tropical and northern hemisphere midlatitude locations that are subject to different meteorological and CO source conditions. The selected airports are Atlanta (USA), Cairo (Egypt), Frankfurt (Germany), Houston (USA), Khartoum (Sudan), Lagos (Nigeria), Los Angeles (USA), Nagoya (Japan), New Delhi (India), New York (USA), Tel Aviv (Israel) and Tokyo (Japan). Again, the sampling frequency among the airports is not the same throughout the period. Similar to the results shown in Fig. 4, in Fig. 5 we notice good agreement. Agreement between the trajectory mapped and the in situ measurements for different locations and seasons across the globe is generally good in the free troposphere. There are larger differences below 2 km where trajectories have larger errors predominantly due to complex dispersion and turbulence in the planetary boundary layer [Stohl and Seibert, 1998]. However, the overall agreement between 2 and 10 km is very good with biases again within 20%. As in previous studies using this method, the largest differences are seen where other sources of data are distant. The smallest overall bias is seen at Frankfurt, even

though the exclusion of Frankfurt data removes nearly 1/3 of the total number of profiles. Apparently data from nearby airports such as Munich (Germany) and Brussels (Belgium) map accurately to the Frankfurt location. The consistency of these validation tests suggests that the trajectory-mapped dataset provides a reliable picture of the tropospheric CO distribution.

**Fig. 56.** Similar to Fig. 4 (lower panels) but for the seasonal mean relative biases  $[2(\text{Clim-MOZAIC})/(\text{Clim}+\text{MOZAIC})]$ , expressed in %, between trajectory-mapped and MOZAIC-IAGOS in situ profiles for the period from 2001 to 2012. In each panel, different colors indicate different seasons: December-February (blue), March-May (green), June-August (red) and September-November (cyan). The selected airports are representative of different meteorological and source conditions across the globe. N, lat and lon are the number of profiles, latitude and longitude of each airports.

### 3.3 Comparison with the MOZAIC-IAGOS in-situ for Upper Troposphere

We can also compare the trajectory-mapped profile data and MOZAIC-IAGOS in situ global CO data at cruise altitudes between 8 and 12 km. The right panels of Fig. 67 show the global seasonal mean (December-February, March-May, June-August and September-November) distribution of CO in the upper troposphere (within 60 hPa below the tropopause) for the period from 2003 to 2011. The figure clearly shows the seasonal cycle of CO with seasonal maximum in the northern hemisphere (NH) spring (MAM) and peak CO values in the southern hemisphere (SH) spring (SON). Elevated CO levels in the upper troposphere are generally seen over the areas where there is strong biomass burning (central Africa, southern Africa and South America). The figure also reveals that high CO emissions are observed over eastern China in MAM primarily due to a rise in coal use (Boden et al., 2009; Gregg et al., 2008; Tie et al., 2006) and an increasing number of vehicles (Cai and Xie, 2007).

The left panels of Fig. 67 show the trajectory-mapped global seasonal variation of CO for December-February, March-May, June-August and September-November climatology 2001-2012 at altitudes between 7 and 9 km above sea level. The trajectory-mapping yields more data over the oceans and NH high latitudes in Fig. 6 than is seen in CO maps cited above. However, major regional features of the global CO distributions for different seasons are clearly evident in both figures. The figures show seasonal high CO values in spring in both hemispheres and elevated CO levels over regions where there is intensive biomass burning (central Africa, southern Africa and South America) and anthropogenic emissions (eastern China are strong sources). Comparable CO values are noticeable from the figures over the Northern Atlantic Ocean, although the trajectory-mapped data appear high over as well high-elevation areas as like Greenland and the Himalayas. This may be due to over-correction of trajectories for terrain

1 ~~differences. Such an~~ Overall, ~~the good~~ qualitative agreement between the trajectory-mapped  
2 CO and MOZAIC-IAGOS in situ CO cruise data ~~result suggests that the trajectory-mapped CO~~  
3 ~~dataset performs well appears very good, even~~ in remote areas ~~as well~~.

6 **Fig. 67.** Global distribution of seasonal mean trajectory-mapped MOZAIC-IAGOS CO between  
7 7-9 km altitudes above sea level for the period from 2001 to 2012. ~~Left: Panels (MOZAIC-~~  
8 ~~IAGOS trajectory). Right: and right ( MOZAIC-IAGOS cruise altitude.~~  
9 ~~) panels a, b, c, and d show the seasonal mean of CO for December February, March May, June-~~  
10 ~~August and September November from top to down, respectively.~~

### 11 3.4 NOAA CO vertical profiles

12 The vertical in situ CO profiles acquired through NOAA's flask sampling program have been  
13 extensively utilized previously for validations of CO measurements of MOPITT [Emmons et al.,  
14 2004; Emmons et al., 2009; Deeter et al., 2010; Deeter et al., 2013]. Typically 12–15 flask  
15 samples are utilized to derive an in situ profile and a single flask is used to sample air at a unique  
16 altitude, providing in situ measurements from near the ground up to about 300–350 hPa. The  
17 flasks are shipped to the Global Monitoring Division of NOAA's Earth System Research  
18 Laboratory (ESRL) for trace gas analysis. Details on procedures of sample collection are found  
19 in Novelli et al. [1992], Lang et al. [1992], and Conway et al. [1994].

20 Figure 6A8 shows comparisons between NOAA in-situ data and the trajectory-mapped  
21 MOZAIC-IAGOS CO climatology, for altitude ranges of 0-2, 2-4, 4-6 and 6-8 km The  
22 comparison uses for all available flask data (1940 profiles for the period from 2001-2012).  
23 NOAA CO data points are matched with the corresponding grid cell ( $5^{\circ} \times 5^{\circ} \times 1$  km) of the  
24 monthly climatology, for the same year and month. If the monthly CO value for a particular grid  
25 cell is missing, the seasonal mean (if it exists) of the trajectory-mapped CO climatology- (2001-  
26 2012) is used for the comparison. Above 2 km agreement is fairly good, considering that the  
27 comparison is between point measurements and monthly averages over a large volume. The  
28 positive bias below 2 km is probably due to the effect of urban sources of CO since airports are  
29 located close to cities. In general, MOZAIC-IAGOS CO measurements at takeoff and landing  
30 are above background. Their "airport effects" decreases rapidly as can be from the figure for  
31 higher altitudes. Their decrease is not only because the aircraft ascends above the boundary  
32 layer, but also samples over 150-400 km in distance as the aircraft ascends to, or descends  
33 from, cruise altitude.



Fig. 6A8 CO mixing ratio comparison between trajectory-derived and NOAA flask data for the period from 2001-2012, for four altitude ranges. Bias is calculated as the mean of the differences in %,  $[2(\text{NOAA}-\text{Clim})/(\text{Clim}+\text{NOAA})]$ , of all data points. The blue line is the line of best fit, the red line is the 1:1 line, N is number of data pairs, and R is the correlation coefficient. Monthly trajectory mapped CO data are used for the comparison, or seasonal mean values if the monthly mean value for a particular grid cell is not available.

#### 4 Trajectory-mapped MOZAIC-IAGOS Versus MOPITT

This section is devoted to comparing the trajectory-mapped MOZAIC-IAGOS CO dataset with the extensively validated product from the MOPITT instrument onboard the NASA Terra satellite, which has been operating continuously since March 2000 (Drummond and Mand, 1996; Edwards et al., 1999). Global comparison ~~was~~is made for both CO profiles and CO total column for different time periods.

##### 4.1 Comparison with MOPITT CO profiles

As described in Section 2.4, in order to make a rigorous comparison with MOPITT data, the climatology profiles are first transformed using the corresponding MOPITT a priori profiles and averaging kernels via Eq. (2). Figure ~~2-3~~2-3 shows examples of retrieved CO profiles ( $x_{\text{ret}}$ ), together with the original climatology ( $x$ ) and the a priori profiles ( $x_a$ ).

~~When examining the comparison between the MOPITT CO retrievals and the trajectory-mapped CO profile it is useful to keep in mind the shapes and magnitudes (or areas) of the averaging kernels. For example, the 100 and 1000 mbar kernels are typically less peaked than the other pressure levels. Consequently, the generally broad and weak averaging kernels for the 100 and 1000 mbar levels demonstrate that a significant fraction of the information used in the retrieval is from the a priori profile or CO and from other layers altitudes or both. Figure 2-3 also cautions that the transformed trajectory-mapped MOZAIC-IAGOS CO is closer to both the MOPITT CO retrievals and a priori profiles when there is less information from the measurement. Furthermore, as can be seen from Fig. 2, the MOPITT retrievals are not able to resolve the finer scale vertical structure of the trajectory mapped CO profiles. The departures of the retrieved CO VMR from the trajectory mapped VMRs at some pressure levels are as large as 60 ppb. In the lower troposphere the MOPITT CO retrieval profile is positively biased (Deeter et al., 2014), whereas the bias is negative in the upper troposphere. In Fig. 23, we have used only the dayside retrievals from MOPITT as the dayside retrievals have the maximum information content (Deeter et al., 2004). The MOPITT V6 L3 retrievals, which have been regridded to 5° resolution, are used in this analysis.~~

Figure 7-9 shows profile-comparisons between MOPITT retrievals and the MOZAIC-IAGOS climatology for global CO data at pressure levels 900 hPa, 700 hPa, 500 hPa, and 300 hPa. The slopes-biases and correlations between MOPITT CO retrievals-VMR and the CO climatology (after applying the averaging kernels and the a priori profiles) for different levels are indicated in the each figureplot. The different dot colors shown in Fig. 7 stand for different latitude bands: 23.5-66.5° S (SH extratropics), 23.5° S-23.5° N (tropics), 23.5-66.5° N (NH extratropics). The same figure shows that there are clearly two distinct clusters of dots in Fig. 7a-9a and 7b-9b, and the high CO VMRs values seen here are from the tropics, with a very few very little small number from the NH extratropics. The enhanced CO values may have originated from anthropogenic sources and/or biomass burning; however, identifying individual sources is beyond the scope of this paper. Recent work by Ding et al. (2015) shows the association of enhanced CO in the free troposphere with the uplifting of CO from biomass burning and anthropogenic sources.

MOPITT and trajectory-mapped MOZAIC-IAGOS CO climatology mixing ratios are well-correlated with correlation coefficients of 0.7 or higher, for daytime data over both land and ocean. However, Fig. 7-9 also reveals significant biases between MOPITT retrievals and the trajectory-mapped MOZAIC-IAGOS CO climatology (geometric) altitudes above the 700 hPa pressure level above 700 hPa. Although in Fig. 7-9 we have chosen to show biases for January DJF winter 2001-2012, the same analysis for other months and time periods seasons yields similar results.

**Fig. 79.** Comparison results for January-DJF (December, January, February) 2001-2012. MOPITT CO retrievals at 900 (a), 700 (b), 500 (c) and 300 (d) hPa are plotted against trajectory-mapped MOZAIC-IAGOS CO climatology profiles that have been transformed using the MOPITT averaging kernels and a priori data. The red line is the 1:1 line, the blue line is the line of best fit,  $N$  denotes the total number of data points,  $R$  is the correlation coefficient,  $RMS$  is root mean square error in ppbv and  $Bias$  is the relative bias between them in %. In each panel, the different color dots show for latitude bands: tropics (cyan), NH extratropics (black) and SH extratropics (blue). group different latitude bands: 23.5-66.5° S (SH extratropics), 23.5° S - 23.5° N (tropics) and 23.5-66.5° N (NH extratropics). In this study, we have used the monthly MOPITT V6 L3 TIR/NIR daytime product.

These large differences are surprising. MOPITT seems to underestimate CO VMR by as much as 21% against the trajectory mapped MOZAIC IAGOS CO climatology at 500 hPa. This result is significantly different from since previous work such as Deeter et al. (2014, 2013, 2010) and Emmons et al. (2004, 2007, 2009). Most of these examined earlier versions of the MOPITT L3 L2 product, although Deeter et al. (2014), who also use the MOPITT L3 V6 product; and

NOAA flask data (among other sources), and reported biases -varying from -5.2% at 400 hPa to 8.9% at the surface. These results are not dissimilar to our comparison in Figure 6A8, and would suggest a difference of about 5% between MOPITT and the trajectory-mapped climatology, with the climatology being higher primarily due to the airport effect. Although the validation data sets are not identical (owing primarily to incomplete global coverage of the MOZAIC-IAGOS product), the relative bias of 22% at 500 hPa seems excessive. In all cases the validation data consisted of flask samples taken by NOAA aircraft. In order to eliminate the possibility that trajectory errors might be contributing to the this bias we find with the MOZAIC-IAGOS CO dataset, we have also compared MOZAIC-IAGOS in situ CO profiles against MOPITT retrievals. As an example in Fig. 810, we display the comparison between MOZAIC-IAGOS in situ CO profiles at Frankfurt (Germany) and MOPITT CO retrievals, which have been regridded to 5° resolution, over Frankfurt from MOPITT overpasses. The MOZAIC-IAGOS in situ aircraft CO values have been transformed using the MOPITT averaging kernels and a priori data, for the period from December 2001- December 2012. MOPITT and MOZAIC-IAGOS are again strongly correlated, and biases at 500 hPa and 300 hPa are large, and in fact very similar in magnitude to those with respect to the trajectory-mapped MOZAIC-IAGOS CO dataset. This implies that the differences at 500 and 300 hPa are not a result of the trajectory mapping.

**Fig. 810.** Same as Fig. 7-9 but MOPITT CO retrievals at 900 hPa (a), 700 hPa (b), 500 hPa (c), and 300 (e) hPa are plotted against MOZAIC-IAGOS CO in situ profiles that have been transformed using the MOPITT averaging kernels and a priori data. The in situ profiles are monthly means from 2001-2012 (Frankfurt, Germany). Outliers (CO mixing ratios more than 1.5 standard deviations from the mean at each pressure level) have been removed, which improves the correlation coefficient at 300 hPa but makes no significant change in other derived parameters.

A global comparison between the trajectory-mapped MOZAIC-IAGOS climatology and MOPITT at 600 hPa is displayed in Fig. 911. As can be seen, from the same figure both datasets capture major features of the CO distribution, particularly anthropogenically polluted (i.e., northeast China) and biomass burning (i.e., west Africa, central Africa, South Africa and central America) regions. The CO-rich air in the lower troposphere over west Africa, where biomass burning fires are active, is convectively lifted vertically upward to the upper troposphere where it disperses over the African tropics towards the east coast of South America and the south Arabian peninsula (Edwards et al., 2003). Indeed, the transport toward South America is much clearer. In Over southern Africa and southeast Asia, where there are strong sources, In this region, and in general at 600 hPa, higher CO VMRs are measured found by the MOZAIC-IAGOS mapping than by MOPITT.

Over southeast Asia, MOZAIC IAGOS detects highly polluted air masses. In these areas MOZAIC IAGOS also measures higher CO than MOPITT. Comparison of the panels for DJF with those for SON of Fig. 9 also show that the NH CO VMRs are much higher during December-February than September-November (a result of the difference in OH, as noted above) and the latitude gradient in December-February is higher than in September-November. This is because in the SH the seasonal peak in CO occurs in September-November. This comparison also reveals a shift of the biomass burning from central Africa to South Africa and central America. Both datasets capture this, although the TIR/NIR product offers the greatest sensitivity to CO in the lower troposphere (Deeter et al., 2014). MOZAIC IAGOS shows higher CO concentrations in these regions than MOPITT. On the other hand, Liu et al. (2005) suggested that since MOPITT (V3-L2) has low sensitivity to CO in the lower troposphere, the CO VMR estimated may only be a lower bound. The same authors noted that fires can be missed if not large enough or if they do not coincide with the MOPITT overpass time, or both. The presence of clouds is also another limitation for missing data.

**Fig. 911.** Global distribution of the seasonal mean trajectory-mapped MOZAIC-IAGOS CO climatology (left panels), after transformation with the MOPITT a priori profiles and averaging kernels matrix, and MOPITT CO retrievals (right panels). CO mixing ratio (ppbv) as a function of latitude and longitude at 800 (a-d) and 600 (e-h) hPa pressure levels. Data are binned at 5°x5° in latitude and longitude for the period from 2001-2012. The CO mixing ratios shown in panels: (a, b) at 800 hPa for DJF, (c, d) at 800 hPa for SON, (e, f) at 600 hPa for DJF and (g, h) at 600 hPa for SON.

Figure S2 shows global maps of percentage differences between MOPITT and the transformed trajectory-mapped MOZAIC-IAGOS CO climatology at 800 and 600 hPa pressure levels for DJF and SON 2001-2012. Differences are generally less than  $\pm 20\%$  at 800 hPa, with a negligible overall bias, but larger at 600 hPa, with MOPITT on average 10-20% higher-lower, except for a few few places over the Caribbean, southeast Asia and central Africa.<sup>22</sup> Generally, the comparisons of the CO profiles of the transformed trajectory-mapped MOZAIC-IAGOS and MOPITT for both grid cells as well as zonal mean for different latitude bands show a consistent, significant bias: MOPITT is lower from about 700 hPa to 300 hPa, but shows a negligible bias in the lowermost troposphere. Above 300 hPa, they seem to agree better, although this may be partly due to the fact that the retrieved CO values in this region are highly influenced by the MOPITT a priori data for both cases.

#### 4.2 Comparison with MOPITT CO total column values

CO total column amounts are retrieved from the MOPITT observations in addition to the profile retrievals. The retrieved CO total column  $c_{ret}$  (a scalar) is related to the retrieved profile  $x_{ret}$  (a vector) through the linear relation

$$c_{ret} = t^T x_{ret} \quad (3)$$

where  $T$  indicates the transpose operation and  $t$  is the total column vectors. The CO total column averaging kernel can be calculated from the profile averaging kernels by

$$a = t^T A \quad (4)$$

The column operator simply converts the mixing ratio for each retrieval level to a partial column amount. Using the hydrostatic relation, the operator  $t$  is expressed as

$$t = 2.120 \cdot 10^{13} \Delta p \quad (5)$$

Equation (5) is expressed in molecules/cm<sup>2</sup>/ppbv and  $\Delta p$  is the vector of the thicknesses of the retrieval pressure levels (in hPa). The interfaces of the retrieval layers are set at the surface, top of the atmosphere, and the midpoints between the standard nine retrieval levels. Determination of  $\Delta p$  required in Eq. (5) has to be made individually for each retrieval because of the variability of the surface pressure. The boundaries of the imaginary layer associated with each level are located at the pressure midpoints between the levels in the grid.

For example, for a surface pressure of 950 hPa, the fixed retrieval pressure grid levels along with surface pressure would be (950, 900, 800, 700, 600, 500, 400, 300, 200, 100) hPa. Hence the corresponding  $\Delta p$  values would be (25, 75, 100, 100, 100, 100, 100, 100, 100, 100) hPa. Column amounts are calculated from the in situ profiles according to Eq. (6) to validate the CO total column retrievals.

In the same manner as we have done for the retrieved CO profiles, the retrievals of CO total column  $c_{ret}$  may be compared against total column values derived from in situ profiles  $x$ . Utilizing Eq. (2), the retrievals of the total CO column  $c_{ret}$  found in Eq. (3) can be rewritten alternatively as

$$c_{ret} = c_a + a(x - x_a) \quad (6)$$

where  $c_a = t^T x_a$  is the a priori total column value corresponding to the a priori profile  $x_a$ ,  $a$  is the CO total column averaging kernel and  $x$  is the in situ profile.

We have calculated the global total CO columns for both the MOZAIC-IAGOS CO climatology (using the MOPITT a priori and averaging kernels by applying Eq. (6)) and for MOPITT CO retrievals and compared different regions of the globe and different times-time intervals from 2001-2012. The comparisons between the climatology and the MOPITT observations agree well,

typically to within 10%. For most regions the MOPITT CO total columns are 10-20% slightly higher than the trajectory-mapped MOZAIC-IAGOS CO climatology total columns, with larger differences while in high CO source regions MOPITT seems to underestimate CO emissions. The SH shows a distinct latitude gradient, which is not evident in the NH. This is likely related to the existence of major CO sources in the NH and the absence of large sources of emission in the SH. Nighttime CO observations of MOPITT have not been validated and appear subject to larger bias (Heald et al., 2004). Hence, we use the daytime data for comparison.

Figure 10-12 shows global total column CO for August 2002, December 2005, December 2011 and August 2012 four seasons. From Fig. 10-12 it is clear that MOPITT and the climatology are similarly able to capture the CO spatial variability. In August 2002 and 2012 NH autumn, elevated total column CO is seen over South America, southeast Asia and west African which is due primarily to agricultural biomass burning in the regions. In both months, we see high total column CO over southeast Asia and west Africa. High total column CO is also seen in all seasons over eastern China, which is one of the major emission regions in the world. Northern hemispheric total columns are much higher than those in the southern hemisphere, and CO is somewhat more abundant in the NH winter (December), which is reasonable expected due to the lower amounts of hydroxyl radical (OH) that are present in the troposphere in that season (reduced oxidizing capacity). Difference plots for the CO maps shown Fig. 10-12 are shown in Figure S3. Generally, the MOPITT CO total column retrievals are slightly higher than the trajectory mapped MOZAIC-IAGOS CO climatology.

**Fig. 1012.** Global total column CO from the transformed trajectory-mapped MOZAIC-IAGOS climatology and MOPITT data for August 2002, December-February, December 2005, March-May, December 2011, June-August and August-September-November 2001-2012. Data are averaged in 5°x5° latitude- longitude bins.

Figure S3 shows global difference plots for the CO maps shown Fig. 10. Biases generally lie within ±20%, and the global mean bias between the MOPITT and MOZAIC-IAGOS CO climatology total columns is typically about 5% or less. While overall bias shows MOPITT to be higher, it is also evident that the trajectory mapped MOZAIC-IAGOS climatology is typically higher near major sources (eastern China, west central Africa and western South America) as well as over some areas of the oceans where aircraft data are not available. The negative biases near major sources are probably due to the limited vertical resolution of MOPITT as previously noted.

Similar results are found for other years (Fig. 1413). This figure shows scatter plots of retrieved MOPITT CO total columns against the transformed trajectory-mapped MOZAIC-IAGOS climatology for August 2008, December 2008, February 2009, March 2009, May 2009, August 2009, June 2010, August 2010 and December 2010, September 2011, November 2011, 2012 the same periods shown in Fig. 1012. MOPITT and the trajectory mapped climatology generally show strong correlations are strong except in SON 2001-2012, and average biases of less than 2012-165%, with MOPITT the trajectory MOZAIC-IAGOAS is higher most cases. This is consistent with previous work, which also However, previous shows positive total column retrieval bias against aircraft data (Deeter et al., 2014, 2013; Emmons et al., 2009, 2007). The trajectory mapped climatology high bias might be in part associated with the effects of urban sources of CO since all airport effect; however the averaging kernels (Fig. 23) are not very sensitive to CO in the boundary layer. s are located near major urban centers.

**Fig. 1413.** Global MOPITT CO column retrievals versus transformed trajectory-mapped MOZAIC-IAGOS CO climatology column for the months and years shown above four seasons. The mean difference in %bias is calculated as the difference for each grid cell,  $[2(MOPITT - Clim)/(Clim + MOPITT)]$ , is calculated for each pixel and then averaged over all pixels grid cells. The blue line is the line of best fit, the red line is the 1:1 line and the correlation coefficient ( $R$ ), total number of data points ( $N$ ) and root mean square error (RMS) are given indicated.

## 5 Results

### 5.1 Global distribution of MOZAIC-IAGOS CO climatology

As an example, Fig-Figure 12-14 shows the monthly mean CO VMR between 4 and 8 km altitude above sea level for the four seasons (i.e., December 2008-February 2009, March 2009-May 2009, June 2009-August 2009 and September 2009-November 2009) during 2001-2012. The climatology is able to capture the CO spatial variability fairly well: the northern hemispheric concentrations are much higher, and the biomass burning peaks are clearly visible for the NH winter and spring seasons. The climatology shows more abundant CO in the NH during these seasons. This is due primarily to lower OH levels during the cold season which permits a longer lifetime for CO, although there also appears to be an additional source in eastern Asia. Enhanced CO concentration is observed in the tropical regions where wildfire burning is typical during the December-January-February season April, like west Africa and a large part of central Africa (Sauvage et al., 2005, 2007). At southern mid-latitudes between South America, southern Africa and Australia, we observe high CO from September to November, during the agricultural burning season. This is accompanied by enhanced ozone in the same region (e.g. Ding et al., 2015; see also Sect. 5.2), produced via reactions R1-R5 and similar. Although Fig. 12-14 shows a 12-year global map, the strong



enhanced CO over these regions (west Africa, South America, and southeast Asia) is clearly observable as an annual feature with significant interannual variability.

Furthermore, Fig. 12 allows us to examine the annual variation of the global distribution of CO between 4 and 8 km altitudes above sea level. Despite the limited MOZAIC-IAGOS data in the SH, the seasonal cycle of CO is clearly shown in both hemispheres. The greatest change of CO from north to south occurs around the tropics in February-April when CO levels are greatest in the NH. The reverse gradient appears with a sharp decrease across the tropics in September-October when CO levels peak in the SH. High CO levels are seen in August between Southeast Africa and Southwest Australia, which is as a result of the long range transport of CO produced from biomass burning in the tropical areas (i.e., southern Africa).

**Fig. 1214.** Global monthly mean CO distribution from the trajectory-mapped MOZAIC-IAGOS CO VMR as a function of latitude and longitude for January-December 2001-2012 and altitudes between 4-8 km a.s.l. The data were averaged with a bin size of  $5^{\circ} \times 5^{\circ}$  latitude and longitude.

## 5.2 Zonal distribution of MOZAIC-IAGOS CO climatology

### 5.2.1 Seasonal variation

**Fig. 1315.** Zonally averaged monthly variation of CO for the latitude bands  $45^{\circ}\text{S}$ - $45^{\circ}\text{N}$  (a),  $23.5^{\circ}\text{S}$ - $23.5^{\circ}\text{N}$  (b),  $23.5$ - $66.5^{\circ}\text{N}$  (c) and  $23.5$ - $66.5^{\circ}\text{S}$  (d). Monthly mean CO VMRs and total columns were calculated for the period 2001-2012. The CO mixing ratios are shown, for altitude ranges 0-2 km, 2-4 km, 4-8 km and 8-12 km, as well as total column (TC) a.s.l. The abscissa is monthly mean of CO covered during 2001-2012.

In Fig. 13, data are grouped in three bands representing the NH extratropics (Fig. 13e), the SH extratropics (Fig. 13d), the tropics (Fig. 13b) and for latitude band  $45^{\circ}\text{S}$ - $45^{\circ}\text{N}$  (Fig. 13a). The zonal mean trajectory mapped MOZAIC-IAGOS CO climatology for these latitude bands is shown for the altitude ranges 0-2 km, 2-4 km, 4-8 km and 8-12 km.

As can be seen from Fig. 1315, CO shows distinct seasonal cycles in both hemispheres. In the NH extratropics (Fig. 13e15c), maximum CO VMR is observed in February-April following a steady increase during fall and winter. This is followed by a rapid decrease giving rise to the lowest CO levels in July-September-August. The seasonal decline of CO VMR in summer shows the typical seasonal pattern of CO in the NH driven by OH increase during this time (Yurganov

et al., 2008; Novelli et al., 1998). In the SH extratropics (Fig. 13d15d), CO levels peak in September-October. This is consistent with previous studies by Novelli et al. (1998). In the SH, the annual CO maximum is earlier at lower altitudes. Rinsland et al. (2002) suggested this phenomenon to be associated with the vertical and horizontal CO dispersion away from the biomass burning region in the tropics. Moreover, CO shows greater seasonal variability, particularly at higher altitudes, in the SH than in the NH. This can also be seen in Fig. 12. The seasonal CO cycle in the tropics (Fig. 13b15b) and for latitude band 45°S-45°N (Fig. 13a15a) both display a July minimum, and a secondary maximum in October while the primary maximum is in late NH winter/early spring. The CO cycle in both hemispheres is controlled by seasonal variations of OH, as OH is the major CO sink (Logan et al., 1981; Bergamaschi et al., 2000; Novelli et al., 1998) and the space-time distribution of its sources (Novelli et al., 1998), in particular the biomass burning either in the Tropics (largest fires occur in austral Africa and South America in SON) or to a lesser degree at boreal latitudes (largest fires in June-July-August), and anthropogenic sources at northern mid-latitudes.

Figure 14-16 shows zonal mean latitude-time cross-section plots of CO VMR at 2.5 km, 4.5 km, 6.5 km, 8.5 km, 10.5 km and 12.5 km altitudes for the period 2001-2012. The latitude-time cross-section shows the seasonal cycle of zonal mean CO for different altitudes, as seen in the previous figures, and also the variation of the interhemispheric CO VMR gradient throughout the year. The strongest interhemispheric gradient occurs in March, at low altitude, and the smallest gradients are seen in northern summer. The gradient in NH spring reverses at higher altitudes, and in NH fall where it is especially strong at higher altitudes. Plots 14e, f also clearly show the weak seasonal cycle in the NH upper troposphere compared to that in the SH.

**Fig. 1416.** Seasonal variation of zonal monthly mean trajectory-mapped MOZAIC-IAGOS CO climatology at 2.5 (a), 4.5 (b), 6.5 (c), 8.5 (d), 10.5 (e) and 12.5 (f) km altitudes a.s.l. for the period 2001-2012. The zonal mean data are averaged in 5° latitude intervals.

### 5.3.2 Vertical distribution

Figure 15-17 illustrates the variation of CO with altitude for the seasons in which we observe maximum CO levels in both the SH and NH (i.e., MAM and SON). The seasons demonstrate the greatest CO VMRs are found at lower altitudes in both hemispheres, although. Even though CO declines with altitude in both hemispheres, it does so faster in the NH than the SH. This which results in a decrease in the strength of the interhemispheric gradient (SH to NH) with altitude. This result is consistent with Edwards et al. (2006) who suggested that in the absence of continued CO input from the source regions (i.e., biomass burning in southern Africa and South America), the aged CO is gradually distributed vertically throughout the troposphere in the SH.

In fact, in regions where there is deep convection this leads to an enhanced CO concentration in the upper troposphere, as can be seen on the right-hand side of Fig. 45-17 and in Fig. 4618d. Moreover, Liu et al. (2006) showed large horizontal CO gradients in association with vertical and horizontal transport of air originated from with different chemical signatures of origin.

~~The z~~onal CO mean vertical profiles for February, April, July and September, averaged for 2001-2012 over the latitude bands 23.5-66.5°N (NH extratropics), 23.5-66.5°S (SH extratropics) and 23.5°S-23.5°N (tropics), are shown in Fig. 4618. ~~The results are displayed for latitude bands 23.5-66.5°N (NH extratropics), 23.5-66.5°S (SH extratropics) and 23.5°S-23.5°N (tropics).~~ The CO profiles show strong seasonal and latitudinal variability primarily in the NH extratropics. The largest VMRs of CO occur at lower altitudes in the NH extratropics in February and April but the strong decline with altitude causes CO VMRs to be higher in the SH at high altitudes than in the NH. ~~In the SH in February, April, July and September, there is little variation of CO with altitude. This is due to the sampling of the lower most stratosphere in the NH much more frequently than in the SH.~~ The trajectory-mapped CO in the SH extratropics is mainly representative of the tropics, while unlike in the NH extratropics ~~where~~ there are many CO measurements north-poleward of 40°N. This implies that sampling of the lowermost stratosphere will be more frequent in the NH than in the SH. The altitude gradients are similar in July and September, with CO levels in September in the SH higher than those in the NH. This is typically the influence of tropical biomass burning in South America and austral Africa, which are the two regions most represented in the climatology in the SH. In the tropics, CO VMRs show a rapid decrease with altitude in the lower troposphere but above approximately 4-5 km changes with altitude are minor.

**Fig. 4517.** Global distribution of seasonal (the NH spring and fall) mean trajectory-mapped MOZAIC-IAGOS CO climatology as a function of latitude and longitude for altitudes 1.5, 3.5, 5.5 km, 7.5 km and 9.5 km a.s.l. The left and right columns show average CO VMRs for March-April-May and September-October-November, 2001-2012. The data are averaged with a bin size of 5°x5° latitude and longitude.

**Fig. 4618.** Monthly mean profiles of CO from the trajectory-mapped MOZAIC-IAGOS CO climatology for February ~~(a)~~, April ~~(b)~~, July ~~(c)~~ and September ~~(d)~~ averaged for 2001-2012. The

different colors represent CO mean VMR for the latitude bands 23.5-66.5°N (blue), 23.5-66.5°S (green) and 23.5°S-23.5°N (red).

## 6 Applications

### 6.1 Global variation and trends of CO

The smoothed time series of the NH extratropical zonal mean CO VMR at 900, 700, 500, and 300 hPa for the trajectory-mapped MOZAIC-IAGOS dataset 2001-2012 is shown in Fig. 1719. For purposes of comparison we also show data from MOPITT and from the mapped MOZAIC-IAGOS dataset transformed with the MOPITT averaging kernels. Gaps in the figure occur whenever one data source is missing. The gaps in June-July 2001 and August-September 2009 were due to a cooler failure of the MOPITT instrument. MOZAIC-IAGOS began CO measurement in December 2001 and there were only partial data available in 2010 and 2011. The observations show an annual late winter or springtime peak in the NH extratropical zonal CO loading each year, in conjunction with low wintertime OH levels. The same interannual cycle of CO is captured by both trajectory-mapped MOZAIC-IAGOS (transformed and untransformed) and MOPITT. They appear to track short-term changes equally well. However, while all show a modest decline in the lower troposphere particularly until about 2008-2009 (and thereafter which CO VMR seems to level off), in accordance with the trends found by Worden et al. (2013), in the upper troposphere MOPITT shows a modest increase, and It also shows a significant bias with respect to the trajectory-mapped MOZAIC-IAGOS data that decreases with time. Although the untransformed trajectory-mapped MOZAIC-IAGOS CO values show a significant difference against the transformed data in the lower troposphere, they seem to agree well at higher levels. However, the untransformed trajectory-mapped MOZAIC-IAGOS data shows higher CO levels compared to than MOPITT CO retrievals for at all levels.

**Fig. 1719.** Zonally averaged time series of monthly mean CO VMR, at individual levels and total columns, as retrieved measured by MOPITT CO retrievals and from the trajectory-mapped MOZAIC-IAGOS CO climatology (transformed and untransformed) and transformed using MOPITT's averaging kernels for the latitude band 23.5°-66.5° N.

Laken and Shahbaz (2014) found increasing CO trends over widespread regions of South America, Mexico, central Africa, Greenland, the eastern Antarctic, and the entire region of India and China from MOPITT data. Figure S4The SH extratropics also shows similar time series similar to those in Fig. 1719 for the SH extratropics, but the negative trend is not as clear as that in the NH due to limited data. The annual springtime peak in the SH zonal CO loading is again visible in all of the time series. This is predominantly associated with dry season biomass burning emissions in South America, southern Africa, southeast Asia, and northwestern

Australia. In later months, the CO resulting from these emissions is generally destroyed by more active photochemistry during the SH summer. At these times, the retrieved zonal CO falls to background levels (around 40-50 ppbv) which are representative of the remote ocean regions where CO production by methane oxidation is the dominant source (Edwards et al., 2006). Biases between MOPITT and MOZAIC IAGOS are again significant at all levels, but lowest in the lower troposphere, and again decrease with time. The untransformed trajectory mapped MOZAIC IAGOS data again show higher CO levels than the transformed CO climatology at all levels.

In Fig. S5, we display the time series of the zonal monthly mean of CO VMR for the tropics. The biases between the MOPITT retrievals and the trajectory-mapped MOZAIC IAGOS in general show the same features as for the extratropics, both in time and vertical levels. The CO values show while the seasonal patterns that combine those seasonal patterns of the NH and SH seen in Figs. 17-19 and S4.

In Sect. 4, we found significant biases between the MOPITT retrievals and the trajectory mapped MOZAIC IAGOS CO dataset. In Fig. S6S4, we display the monthly mean time series for Frankfurt from December 2001--December 2012. As can be seen from the figure, These also show we notice again significant biases, declining with time, between MOPITT and the transformed MOZAIC-IAGOS in situ above 700 hPa, in good agreement with the result shown in Fig. 1719. The biases also appear to decrease similarly with time in the upper troposphere. Furthermore, MOPITT shows a modest increase in CO levels in the upper troposphere while MOZAIC-IAGOS in situ (transformed and untransformed) shows a modest decline, consistent with Petetin et al. (2015), who report a similar decrease over Frankfurt. The MOPITT retrievals and MOZAIC-IAGOS (transformed and untransformed) CO values also for Frankfurt show the same seasonal patterns as the NH extratropics (Fig. 17)19). This comparison indicates suggests that a prominent bias, declining with time, exists between MOZAIC-IAGOS and MOPITT L3 V6 TIR/NIR products.

## 6.2 Global distribution of O<sub>3</sub>-CO correlations

Global O<sub>3</sub> datasets have been developed by trajectory mapping of ozonesonde, aircraft and satellite measurements and validated (Tarasick et al., 2010; G. Liu et al., 2013; J. Liu et al., 2013; Osman et al., manuscript in preparation). The maps show consistent agreement with independent in situ and satellite instruments. As a potential application of such datasets (O<sub>3</sub> and CO maps), we present here the relationship between O<sub>3</sub> and CO. The O<sub>3</sub>-CO correlations were derived from the concurrent measurements of O<sub>3</sub> and CO using MOZAIC-IAGOS.

Since CO is involved in the production and destruction of O<sub>3</sub>, studies of O<sub>3</sub>-CO correlation can offer significant insight into the photochemical origin of air masses (e.g. Parrish et al., 1993; Chin et al., 1994; Zhang et al., 2008; Voulgarakis et al., 2011; Kim et al., 2013). A positive correlation is expected in regions where CO and O<sub>3</sub> are related due to emissions and

photochemistry (for example, downwind of major CO and NO<sub>x</sub> source regions and in the presence of a significant actinic flux). However, during winter, Parrish (1993) observed that O<sub>3</sub>-CO were negatively correlated, presumably due to titration of O<sub>3</sub> by NO. Strong anticorrelation is also expected where stratospheric intrusions are a significant source of O<sub>3</sub>, since CO mixing ratios in the stratosphere are quite low. For a remote maritime site, O<sub>3</sub>-CO correlation would only be expected during periods when the site was downwind of significant CO and NO<sub>x</sub> sources.

Although a quantitative interpretation in terms of O<sub>3</sub> production is complicated by sampling of air masses with varying background mixing ratios (Chin et al., 1994; Mauzerall et al., 1998), the correlation still provides valuable information about anthropogenic influence on O<sub>3</sub>. Figures 19-21 examine the O<sub>3</sub>-CO correlations observed by concurrent O<sub>3</sub> and CO measurements using MOZAIC IAGOS instruments during the period from 2001-2012.

Figure 18 shows the global spatial distribution of O<sub>3</sub> and CO from the trajectory mapped MOZAIC IAGOS climatologies for June-August and September-November of 2001-2012 at 4.5 km above sea level. The right panels of Fig. 18 show significantly enhanced CO and O<sub>3</sub> VMRs in the SH between southern Africa and Australia. In central Africa, where there is strong production of CO as a result of high biomass burning, there appears to be high O<sub>3</sub> concentrations during September-November in anthropogenically polluted and biomass burning regions. In the polluted region of east China O<sub>3</sub> is highest in the summer when photochemical activity is at its peak. The highest values of O<sub>3</sub> in the summertime are seen over the Middle East, north Africa and central Asia. The global spatial distribution of O<sub>3</sub> and CO from MOZAIC IAGOS is generally consistent with previous OMI/AIRS results reported by Kim et al. (2013).

**Fig. 18.** Global distribution of seasonal (NH Winter and Fall) mean concentrations of O<sub>3</sub> and CO from the trajectory mapped MOZAIC IAGOS climatologies as a function of latitude and longitude at 4.5 km altitude above sea level. The data are binned on a 5°×5° latitude and longitude grid.

Correlation coefficients of the trajectory mapped MOZAIC IAGOS O<sub>3</sub> and CO climatology seasonal fields from 2001-2012 are displayed in Fig. 19. The seasonal O<sub>3</sub>-CO correlations for the three month time series (DJF, MAM, JJA, SON) of the O<sub>3</sub> and CO mixing ratios were computed for each grid. Figure 19 shows that in June-August and September-November, the O<sub>3</sub>-CO correlation coefficients in the SH appear to be very strong positive in the southern midlatitudes in winter-spring. This suggests that in the SH winter, spring (and perhaps even in autumn) photochemical O<sub>3</sub> production is more dominant. In general, in the NH the O<sub>3</sub>-CO correlations seem to be fairly positive in all seasons except the scattered low negative correlation coefficients seen in the spring (and perhaps even in autumn). This indicates that photochemical O<sub>3</sub> production clearly dominates most of the year at lower altitudes.

**Fig. 19.**  $O_3$ -CO correlation coefficients of seasonal means for 2001-2012 from the trajectory-mapped MOZAIC IAGOS measurements at 4.5 km altitude a.s.l. The top left, top right, bottom left and bottom right panels are the  $O_3$ -CO correlation coefficients for December-February, March-May, June-August and September-November, respectively.

**Fig. 20.** Same as Fig. 19 but for an altitude of 8.5 km a.s.l.

Figure 20 shows the  $O_3$ -CO correlation coefficients at 8.5 km altitude. In the SH strongly positive  $O_3$ -CO correlation coefficients are notable in all seasons except December-February, which suggests that photochemical  $O_3$  production is dominant here even at this altitude. Strong negative correlations in the NH mid and higher latitudes in December-February and March-May indicate that the stratosphere is a major  $O_3$  source at this altitude. In the NH summer where photochemical  $O_3$  formation is a dominant source of  $O_3$ , positive  $O_3$ -CO correlation coefficients are seen, consistent with previous work by Zahn et al. (2002). Moreover, the same figure shows (see also Fig. 21) that in all four seasons  $O_3$ -CO correlation coefficients in the tropics are positive. This is consistent with model calculations that estimate the  $O_3$  abundance in the tropical upper troposphere originating from the stratosphere to be only 5–15% (Roelofs and Lelieveld, 1997; Lamarque et al., 1999). Some fraction of the extratropical CO may originate as CO transported from tropical biomass burning regions to the extratropics; however Bowman (2006) showed using MOPITT CO data that transport from the tropics to the extratropics is a comparatively slow process while the zonal dispersion of air parcels within the tropics and subtropics is relatively rapid.

As a summary, in Fig. 21 we display the distribution of the zonal mean of the  $O_3$ -CO correlation coefficients from the trajectory mapped CO and  $O_3$  datasets as a function of latitude and altitude for the period from 2001-2012. The figure shows that in the lower troposphere the  $O_3$ -CO correlations have generally positive values as photochemistry is the dominant source of  $O_3$ , and the stratospheric influence is relatively small. In the mid and upper troposphere, the influence of the influx of stratospheric air depends strongly on latitude and season, but it always affects calculated  $O_3$ -CO correlation coefficients. The NH high latitudes show negative correlations in winter, spring and fall, in agreement with previous studies (e.g. Voulgarakis et al., 2011; Parrish et al., 1998). Due to lack of sunlight, these regions do not experience intense photochemistry and are dominated by  $O_3$  destruction or dry deposition or both (Voulgarakis et al., 2011). Even though stratospheric intrusion can drive the negative correlations in the region, it is more frequent in spring (Zhang et al., 2008). In the SH, strong correlations are seen at all altitudes in all seasons except December-February, in agreement with those reported by Kim et al. (2013).



Further division of the climatology into annual averages may provide a global view of CO changes and transport. As CO is involved in both the production and destruction of O<sub>3</sub>, O<sub>3</sub>-CO correlations derived from the trajectory mapped MOZAIC-IAGOS CO and O<sub>3</sub> climatology datasets presented here may provide important insights into the origin of air masses and the budgets of O<sub>3</sub> and CO in the troposphere. Figure 21 demonstrates one aspect of the value of the MOZAIC-IAGOS continuous, long term, global, vertically resolved in situ measurements. Such routine commercial aircraft observations provide valuable information on atmospheric composition that can improve our understanding of global and regional air quality and the potential impact of greenhouse gases on climate change.

**Fig. 21.** Latitude-altitude cross section of zonal seasonal means of the O<sub>3</sub>-CO correlation coefficients for 2001-2012 from the trajectory mapped MOZAIC-IAGOS CO and O<sub>3</sub> climatologies. The top-left, top-right, bottom-left and bottom-right panels are the O<sub>3</sub>-CO correlation coefficients for December-February, March-May, June-August and September-November, respectively.

## 7 Conclusions

We have presented a three-dimensional (i.e., latitude, longitude, altitude) gridded climatology of CO developed by trajectory mapping of global MOZAIC-IAGOS data. This quasi-global climatology dataset offers a complement to global satellite measurements, at significantly higher vertical resolution, that facilitates visualization and comparison of different years and seasons, and offers insight into the global variation and trends of CO. Even though the MOZAIC-IAGOS aircraft data are unevenly distributed both in time and space across the globe, the trajectory-mapped dataset is uniformly distributed on a 5°×5°×1 km grid. The trajectory-based interpolation method confers significant advantages over linear or quadratic interpolation. Major regional features of the global CO distribution are clearly evident in the CO maps for different seasons and altitudes. The trajectory-mapped CO shows distinct seasonal cycles with the CO annual maximum occurring in September-October in the SH, coincident with the tropical biomass burning season (Rinsland et al., 2002), and in April in the NH, while the tropics show distinct maxima in January-February and in October. We note caution that the observed result in the SH is obtained from the limited data we have from the region. The interhemispheric CO gradient is strongest in late winter/early spring, and smallest in northern summer. Time series analysis of the climatology shows that in the NH and the tropics CO is declining with time. This is consistent with the previous studies using ground-based, aircraft and satellite data, such as Petetin et al. (2015), Worden et al. (2013), Laken and Shahbaz (2014) and Novelli et al. (1998). In the SH,

~~due to limited MOZAIC-IAGOS data, a clear CO trend cannot be seen.)~~ The consistency of our findings with those from other global datasets lends increased confidence that the CO climatology dataset derived from trajectory mapping of global MOZAIC-IAGOS data can be used for CO trend studies at regional and global scales.

The trajectory-mapped CO dataset has been validated by comparing maps constructed using only forward trajectories and using only backward trajectories. The two methods show similar global CO distribution patterns. Differences are most commonly 10% or less, and found to be less than 30% for almost all cases. They are typically less than 10% at northern mid-latitudes and less than 20% in the tropics between  $\pm 30^\circ$  latitude, except in the Pacific and Atlantic oceans where it can reach as large as 30%. The dataset has also been validated by comparison against in-situ MOZAIC-IAGOS aircraft measurements, where the data from the validation site are excluded from the trajectory-mapped data. Although the comparison shows larger differences below 2 km, the profiles from the two methods agree very well between 2 and 10 km with the magnitude of bias differences within 20%. ~~A further~~ comparison between the trajectory-mapped result and MOZAIC-IAGOS in situ CO cruise data, ~~which were not included in the trajectory-mapping,~~ shows that major regional features of the global CO distribution for different seasons are clearly evident in both maps and they agree very well ~~qualitatively in regions of overlap~~. This suggests that the trajectory-mapped CO data performs well not only near airports but also in remote areas. Validation was also performed against independent data from the NOAA aircraft flask sampling program. The results suggest small or insignificant biases in the upper troposphere, but positive biases as large as 12% for MOZAIC-IAGOS in the lower troposphere. This is probably due to the “airport effect”, a sampling bias that occurs because commercial aircraft operate from large airports near large cities, with typically elevated CO levels in the boundary layer.

The trajectory-mapped CO dataset has also been extensively compared with MOPITT retrievals. Between 700 and 300 hPa, a prominent bias, declining with time, exists between MOZAIC-IAGOS and MOPITT L3 V6 TIR/NIR products.

~~A small positive bias for CO total column is found, consistent with those previously reported for MOPITT (Deeter et al., 2014, 2013; Emmons et al., 2009, 2007).~~

~~Comparison of similar maps made using the concurrent  $O_3$  measurements by MOZAIC-IAGOS permits some insight into the sources of tropospheric  $O_3$ . The  $O_3$ -CO correlation shows a significant seasonal and latitudinal variation. In the tropics, where the influence by stratospheric air is small, generally positive correlations are seen, as photochemistry is the dominant source of  $O_3$ . In the extratropics, strong negative correlations in the NH winter, spring and autumn indicate that the influx of stratospheric air is a primary source, especially in the upper troposphere, while the picture is mixed in the summer. Strong  $O_3$ -CO correlations are noted in all seasons except December-February over southern Africa, which suggests that photochemistry is generally the predominant  $O_3$  source in this region.~~

~~Such constraints on tropospheric ozone sources can be useful for chemical transport model evaluation, as demonstrated by Kim et al. (2013).~~

~~This study demonstrates one aspect of the value of the MOZAIC-IAGOS continuous, long-term, global, vertically resolved in situ measurements. Such routine commercial aircraft observations provide valuable information on atmospheric composition that can improve our understanding of global and regional air quality and the potential impact of greenhouse gases on climate change. Further division of the climatology into annual averages may provide a global view of CO changes and transport as well as interannual variability. The dataset presented here has the potential to be used for time series and trend analysis, and provides a quasi-global view of CO changes and transport as well as interannual variability. It~~  
will also be useful as model initial fields, and background and boundary fields. It will be especially useful as an improved a priori climatology for satellite data retrieval. The global picture it presents is also expected to be valuable for comparison and validation of model results.  
~~The data are publically available at [ftp://es-ee.tor.ec.gc.ca/pub/ftpd/MOZAIC\\_output\\_CO/](ftp://es-ee.tor.ec.gc.ca/pub/ftpd/MOZAIC_output_CO/).~~

**Acknowledgements.** The authors acknowledge the strong support of the European Commission, Airbus, and the Airlines (Lufthansa, Air-France, Austrian, Air Namibia, Cathay Pacific, Iberia and China Airlines so far) who carry the MOZAIC or IAGOS equipment and perform the maintenance since 1994. MOZAIC is presently funded by INSU-CNRS (France), Météo-France, Université Paul Sabatier (Toulouse, France) and Research Center Jülich (FZJ, Jülich, Germany). IAGOS has been additionally funded by the EU projects IAGOS-DS and IAGOS-ERI. The MOZAIC-IAGOS database is supported by ETHER (CNES and INSU-CNRS). Data are also available via Ether web site <http://www.pole-ether.fr>. We thank the many whose dedication makes such a dataset possible. The MOPITT ~~data were obtained from the NASA Langley Research Center Atmospheric Science Data Center.~~ ~~team is appreciated for their datasets for validation.~~ We ~~acknowledge~~ thank R. Draxler and the NOAA Air Resources Laboratory for the trajectory model HYSPLIT ~~(Hybrid Single Particle Lagrangian Integrated Trajectory Model) from the NOAA Air Resources Laboratory (<http://www.arl.noaa.gov/ready.html>), driven by the and NCEP/NCAR for the global meteorological reanalysis data—data from the NOAA/OAR/ESRL PSD, Boulder, Colorado, USA, at <http://www.esrl.noaa.gov/psd/>.~~ The first author is grateful to the Natural Sciences and Engineering Research Council of Canada (NSERC) and Environment Canada for a research fellowship. ~~Important discussions with Merritt Deeter regarding MOPITT averaging kernels are much appreciated. We thank Paul Novelli and Colm Sweeney of NOAA/Global Monitoring Division and Steven Wofsy of Harvard University/School of Engineering and Applied Sciences for providing the in situ CO profiles.~~

## References

1 Bergamaschi, P., R. Hein, M. Heimann, and P. J. Crutzen, Inverse modeling of the global CO  
2 cycle: 1. Inversion of CO mixing ratios, *J. Geophys. Res.*, 105(D2), 1909  
3 doi:10.1029/1999JD900818, 2000.

4 Boden, T. A., G. Marland, and R. J. Andres, Global, Regional, and National Fossil-Fuel CO<sub>2</sub>  
5 Emissions. Carbon Dioxide Information Analysis Center, Oak Ridge Natl. Lab., U.S. Dep. of  
6 Energy, Oak Ridge, Tenn., doi:10.3334/CDIAC/00001. (Available at  
7 <http://cdiac.ornl.gov/trends/emis/cpa.html>), (last access: 8 September 2015), 2009.

8 ~~Bowman, K. W., Rodgers, C. D., Kulawik, S. S., Worden, J., Sarkissian, E., Osterman, G., Steck,~~  
9 ~~T., Lou, M., Eldering, A., Shephard, M., Worden, H., Lampel, M., Clough, S., Brown, P.,~~  
10 ~~Rinsland, C., Gunson, M., Beer, R., Tropospheric emission spectrometer: Retrieval method and~~  
11 ~~error analysis, *IEEE Trans. Geosci. Remote. Sens.*, 44, 1297–1307, 2006.~~

12 Brook, J.R., T.F. Dann, E. Galarneau, D. Herod and J.-P. Charland, (2014), The State of Air  
13 Quality in Canada: National Patterns, in *Air Quality Management, Canadian Perspectives on a*  
14 *Global Issue*, Springer, Dordrecht, ISBN 978-94-007-7557-2, 43-67, doi: 10.1007/978-94-007-  
15 7557-2

16 Cai, H., and S. Xie, Estimation of vehicular emission inventories in China from 1980 to 2005,  
17 *Atmos. Environ.*, 44(39), 8963–8979, 2007.

18 Carmichael, G. R., Y. Tang, G. Kurata, I. Uno, D.G. Streets, J-H Woo, H. Huang, J. Yienger, B.  
19 Lefer, R.E. Shetter, D.R. Blake, E. Atlas, A. Fried, E. Apel, F. Eisele, C. Cantrell, M.A. Avery,  
20 J.D. Barrick, G.W. Sachse, W.L. Brune, S.T. Sandholm, Y. Kondo, H.B. Singh, R.W. Talbot, A.  
21 Bandy, D. Thorton, A.D. Clarke, and B.G. Heikes, Regional-scale chemical transport modeling  
22 in support of intensive field experiments: Overview and analysis of the TRACE-P observations,  
23 *J. Geophys. Res.*, 108(D21), 8823, doi:10.1029/2002JD003117, 2003.

24 Chameides, W., . L., P.S. Kasibhatla, J. J. Yienger, H . Levy II, and W. J. Moxim, The growth of  
25 continental-scale metro-agro-plexes, regional ozone pollution, and world food production,  
26 *Science*, 264, 74-77, 1994.

27 ~~Chin, M., D. J. Jacob, J. W. Munger, D. D. Parrish, and B. G. Doddridge, Relationship of ozone~~  
28 ~~and carbon monoxide over North America, *J. Geophys. Res.*, 99, 14,565–14,573, 1994.~~

29 Clark H., B. Sauvage, V. Thouret, P. Nédélec, R. Blot, K.Y. Wang, H. Smit, P. Neis, A. Petzold,  
30 G. Athier, D. Boulanger, J-M. Cousin, K. Beswick, M. Gallagher, D. Baumgardner, J. Kaiser, J-  
31 M. Flaud, A. Wahner, A. Volz-Thomas and J-P. Cammas, The first regular measurements of  
32 ozone, carbon monoxide and water vapour in the Pacific UTLS by IAGOS, *Tellus B*, 67, 28385,  
33 <http://dx.doi.org/10.3402/tellusb.v67.28385>, 2015.

1 [Conway, T. J., P. P. Tans, L. S. Waterman K., W. Thoning D., R. Kitzis, K. A. Masarie, and N](#)  
2 [.Zhang, Evidence for interannual variability of the carbon cycle from the NOAA/CMDL global](#)  
3 [air sampling network, J. Geophys. Res.,99, 22,831-22,855, 1994.](#)

4 Crutzen, P. A., A discussion of the chemistry of some minor constituents in the stratosphere and  
5 troposphere, Pure and Applied Geophysics 106±108, 1385-1399, 1973.

6 [Deeter, M. N. \(2002\), Calculation and Application of MOPITT \(Measurements of Pollution in](#)  
7 [the Troposphere\) Averaging Kernels, Available at](#)  
8 [http://www.acom.ucar.edu/mopitt/data/avg\\_krnls\\_app.pdf](http://www.acom.ucar.edu/mopitt/data/avg_krnls_app.pdf)

9 Deeter, M. N., L. K. Emmons, D. P. Edwards, J. C. Gille, and J. R. Drummond, Vertical  
10 resolution and information content of CO profiles retrieved by MOPITT, Geophys. Res. Lett.,  
11 31, L15112, doi:10.1029/2004GL020235, 2004.

12 [Deeter, M. N., MOPITT \(Measurements of Pollution in the Troposphere\) Validated Version 5](#)  
13 [Product User's Guide, National Center for Atmospheric Research. Available at](#)  
14 [http://www.acom.ucar.edu/mopitt/v5\\_users\\_guide\\_beta.pdf](http://www.acom.ucar.edu/mopitt/v5_users_guide_beta.pdf), 2011.

15 [Deeter, M., H.M. Worden, D.P. Edwards, J.C. Gille, and A.E. Andrews: Evaluation of MOPITT](#)  
16 [retrievals of lower-tropospheric carbon monoxide over the United States, J. Geophys. Res., 117,](#)  
17 [D13306, DOI: 10.1029/2012JD017553, 2012.](#)

18 [Deeter, M. N., Edwards, D. P., Gille, J. C., Emmons, L. K., Francis, G., Ho, S.-P., Mao, D.,](#)  
19 [Masters, D., Worden, H., Drummond, J. R., and Novelli, P.: The MOPITT Version 4 CO](#)  
20 [Product: Algorithm Enhancements, Validation, and Long-Term Stability, J. Geophys. Res., 115,](#)  
21 [D07306, doi:10.1029/2009JD013005, 2010.](#)

22 Deeter, M. N., Martínez-Alonso, S., Edwards, D. P., Emmons, L. K., Gille, J. C., Worden, H. M.,  
23 Pittman, J. V., Daube, B. C., and Wofsy, S. C.: Validation of MOPITT Version 5 thermal-  
24 infrared, near-infrared, and multispectral carbon monoxide profile retrievals for 2000–2011, J.  
25 Geophys. Res., 118, 6710–6725, doi:10.1002/jgrd.50272, 2013.

26 Deeter, M. N., Martínez-Alonso, S., Edwards, D. P., Emmons, L. K., Gille, J. C., Worden, H. M.,  
27 Sweeney, C., Pittman, J. V., Daube, B. C., and Wofsy, S. C.: The MOPITT Version 6 product:  
28 algorithm enhancements and validation, Atmos. Meas. Tech., 7, 3623-3632, 2014.

29 Ding, K., Liu, J., Ding, A., Liu, Q. , Zhao, T. L., Shi, J., Han, Y., Wang, H., Jiang, F.:  
30 Uplifting of carbon monoxide from biomass burning and anthropogenic sources to the free  
31 troposphere in East Asia, Atmos. Chem. Phys.15, 2843-2866, doi:10.5194/acp-15-2843-2015,  
32 2015.

33 Draxler, R. R.: HYSPLIT4 user's guide, NOAA Tech. Memo, ERL ARL-230, NOAA Air  
34 Resources Laboratory, Silver Spring, MD, 1999.

- 1 Draxler, R.R., Hess, G.D., An overview of the Hysplit\_4 modeling system for trajectories,  
2 dispersion, and deposition. Australian Meteorological Magazine 47, 295–308, 1998.
- 3 Drummond, J. R., and G. S. Mand, The Measurements of Pollution in the Troposphere  
4 (MOPITT) instrument: Overall performance and calibration requirements, J. Atmos. Oceanic  
5 Technol., 13, 314– 320, 1996.
- 6 Edwards, D. P., Lamarque, J.-F., Attie', J.-L., Emmons, L. K., Richter, A., Cammas, J.-P.,  
7 Gille, J. C., Francis, G. L., Deeter, M. N., Warner, J., Ziskin, D. C., Lyjak, L. V., Drummond, J.  
8 R., and Burrows., J. P.: Tropospheric ozone over the tropical Atlantic: A satellite perspective, J.  
9 Geophys. Res., 108(D8), 4237, doi:10.1029/2002JD002927, 2003.
- 10 Edwards, D. P., C. Halvorson, and J. C. Gille, Radiative transfer modeling of the EOS Terra  
11 Satellite Measurements of Pollution in the Troposphere (MOPITT) instrument, J. Geophys. Res.,  
12 104, 16,755–16,775, 1999.
- 13 Edwards, D. P., G. Petron, P. C. Novelli, L. K. Emmons, J. C. Gille, and J. R. Drummond,  
14 Southern Hemisphere carbon monoxide interannual variability observed by Terra/Measurement  
15 of Pollution in the Troposphere (MOPITT), J. Geophys. Res., 111, D16303,  
16 doi:10.1029/2006JD007079, 2006.
- 17 Emmons, L. K., D. P. Edwards, M. N. Deeter, J. C. Gille, T. Campos, P. N'ed'elec, P. Novelli,  
18 and G. Sachse, Measurements of Pollution In The Troposphere (MOPITT) validation through  
19 2006, Atmos. Chem. Phys., 9, 1795–1803, 2009.
- 20 Emmons, L. K., G. G. Pfister, D. P. Edwards, J. C. Gille, G. Sachse, D. Blake, S. Wofsy, C.  
21 Gerbig, D. Matross, and P. Ne'de'lec, Measurements of Pollution in the Troposphere (MOPITT)  
22 validation exercises during summer 2004 field campaigns over North America, J. Geophys. Res.,  
23 112, D12S02, doi:10.1029/2006JD007833, 2007.
- 24 Emmons, L. K., Gille, J. C., Edwards, D. P., Attie', J.-L., Warner, J., Ziskin, D., Francis, G.,  
25 Khattatov, B., Yudin, V., Lamarque, J.-F., Ho, S.-P., Mao, D., Chen, J. S., Drummond, J.,  
26 Novelli, P., Sachse, G., Coffey, M. T., Hannigan, J. W., Gerbig, C., Kawakami, S., Kondo,  
27 Y., Takegawa, N., Schlager, H., Baehr, J., Ziereis, H., Validation of Measurements of Pollution  
28 in the Troposphere (MOPITT) CO retrievals with aircraft in situ profiles, J. Geophys. Res., 109,  
29 D03309, doi:10.1029/2003JD004101, 2004.
- 30 Fishman, J., and Seiler, W., Correlative Nature of Ozone and Carbon Monoxide in the  
31 Troposphere: Implications for the Tropospheric Ozone Budget, J. Geophys. Res., 88, C6, 3662-  
32 3670, 1983.
- 33 Galanter, M., H. Levy II, and G. R. Carmichael, Impacts of biomass burning on tropospheric CO,  
34 NOx, and Os, J. Geophys. Res., 105, 6633-6653, 2000.

- 1 Granier, C., Bessagnet, B., Bond, T., D'Angiola, A., v. d. Gon, H. D., Frost, G. J., Heil, A.,  
2 Kaiser, J. W., Kinne, S., Klimont, Z., Kloster, S., Lamarque, J.-F., Lioussé, C., Masui, T.,  
3 Meleux, F., Mieville, A., Ohara, T., Raut, J.-C., Riahi, K., Schultz, M. G., Smith, S. J., Thomson,  
4 A., v. Aardenne, J., v. d. Werf, G. R., and v. Vuuren, D. P.: Evolution of anthropogenic and  
5 biomass burning emissions of air pollutants at global and regional scales during the 1980–2010  
6 period, *Clim. Change*, 109, 163–190, doi:10.1007/s10584-011-0154-1, 2011.
- 7 Gregg, J. S., R. J. Andres, and G. Marland, China: Emissions pattern of the world leader in CO<sub>2</sub>  
8 emissions from fossil fuel consumption and cement production, *Geophys. Res. Lett.*, 35, L08806,  
9 doi:10.1029/2007GL032887, 2008.
- 10 Heald, C. L., Jacob, D. J., Jones, D. B. A., Palmer, P. I., Logan, J. A., Streets, D. G., Sachse, G.  
11 W., Gille, J. C., Hoffman, R. N., and Nehrkorn, T.: Comparative inverse analysis of satellite  
12 (MOPITT) and aircraft (TRACE-P) observations to estimate Asian sources of carbon monoxide,  
13 *J. Geophys. Res.*, 109, D15S04, doi:10.1029/2004JD005185, 2004.
- 14 Holloway, T., Levy II, H., Kasibhatla, P., Global distribution of carbon monoxide. *J. Geophys.*  
15 *Res.*, 105, 12123e12147, 2000.
- 16 Hoor, P., Gurk, C., Brunner, D., Hegglin, M. I., Wernli, H., and Fischer, H.: Seasonality and  
17 extent of extratropical TST derived from in-situ CO measurements during SPURT, *Atmos.*  
18 *Chem. Phys.*, 4, 1427–1442, 2004.
- 19 Hubler, G., Montzka, D. D., Norton, R. B., Murphy, P. C., Fehsenfeld, F. C., Liu, S. C., Ridley,  
20 B. A., Walega, J. G., Atlas, E., Grahek, F. E., Heidt, L. E., Merrill, J., Huebert, B. J., and  
21 Bodhaine, B. A.: Total reactive oxidized nitrogen (NO<sub>y</sub>) in the remote pacific troposphere and  
22 its correlation with O<sub>3</sub> and CO: Mauna Loa Observatory Photochemistry Experiment 1988, 25, *J.*  
23 *Geophys. Res.*, 97, 10 427–10 447, 1992.
- 24 [IPCC, 2013 \(IPCC AR5\): Climate Change 2013: The Physical Science Basis. Contribution of](#)  
25 [Working Group I to the Fifth Assessment Report of the Intergovernmental Panel on Climate](#)  
26 [Change \[Stocker, T.F., D. Qin, G.-K. Plattner, M. Tignor, S.K. Allen, J. Boschung, A. Nauels, Y.](#)  
27 [Xia, V. Bex and P.M. Midgley \(eds.\)\]. Cambridge University Press, Cambridge, United](#)  
28 [Kingdom and New York, NY, USA, 1535 pp.](#)
- 29 Jacob, D. J., Crawford, J. H., Kleb, M. M., Connors, V. S., Bendura, R. J., Raper, J. L., Sachse,  
30 G. W., Gille, J. C., Emmons, L., and Heald, C. L.: Transport and Chemical Evolution over the  
31 Pacific (TRACE-P) aircraft mission: Design, execution, and first results, *J. Geophys. Res.*,  
32 108(D20), 9000, doi:10.1029/2002JD003276, 2003.
- 33 Jaffe, D.A., R.E. Honrath, L. Zhang, H. Akimoto, A. Shimizu, H. Mukai, K. Murano, S.  
34 Hatakeyama, and J. Merrill, Measurements of NO, NO<sub>y</sub>, CO, and O<sub>3</sub> and estimation of the



1 ozone production rate at Oki Island, Japan during PEM-West, J. Geophys. Res., 101, 2037-2048,  
2 1996.

3 Kalnay, E., Kanamitsu, M., Kistler, R., Collins, W., Deaven, D., Gandin, L., Iredell, M., Saha,  
4 S., White, G., Woollen, J., Zhu, Y., Leetmaa, A., Reynolds, R., Chelliah, M., Ebisuzaki, W., 30  
5 Higgins, W., Janowiak, J., Mo, K. C., Ropelewski, C., Wang, J., Jenne, R., and Joseph, D.: The  
6 NCEP/NCAR 40-year reanalysis project, B. Am. Meteorol. Soc., 77, 437–471, 1996.

7 Khalil, M. A. K., and R. A. Rasmussen, Carbon monoxide in the Earth's atmosphere: Indications  
8 of a global increase, Nature, 332, 242-245, 1988.

9 Khalil, M. A. K., and R. A. Rasmussen, Global decrease in atmospheric carbon monoxide  
10 concentration, Nature, 370, 639-641, 1994.

11 Kim, P. S., D. J. Jacob, X. Liu, J. X. Warner, K. Yang, K. Chance, V. Thouret, and P. Nedelec,  
12 Global ozone–CO correlations from OMI and AIRS: constraints on tropospheric ozone sources,  
13 Atmos. Chem. Phys., 13, 9321–9335, 2013.

14 Laken, B., Shahbaz, T., Satellite-Detected Carbon Monoxide Pollution during 2000–2012:  
15 Examining Global Trends and also Regional Anthropogenic Periods over China, the EU and the  
16 USA, Climate, 2(1), 1-16; doi:10.3390/cli2010001, 2014.

17 [Lang, P.M., L. P. Steele, L. S. Waterman, R. C. Martin, K. A. Masarie, and E. J. Dlugokencky](#)  
18 [NO AA/CMDL atmospheric methane data for the period 1983-1990 from shipboard flask](#)  
19 [sampling NOAA Tech. Memo., ERL CMDL-4, 88 pp., 1992.](#)

20 ~~[Lamarque, J. F., P. G. Hess, and X. X. Tie, Three dimensional model study of the influence of](#)~~  
21 ~~[stratosphere–troposphere exchange and its distribution on tropospheric chemistry, J. Geophys.](#)~~  
22 ~~[Res., 104, 26,363–26,372, 1999](#)~~

23 Law, K. S., and J. A. Pyle, Modeling trace gas budgets in the troposphere 2. CH<sub>4</sub> and CO, J.  
24 Geophys. Res., 98, 18401–18412, doi:10.1029/93JD01480, 1993.

25 Lelieveld, J., P. J. Crutzen, V. Ramanathan, M. O. Andreae, C. A. M. Brenninkmeijer, T.  
26 Campos, G. R. Cass, R. R. Dickerson, H. Fischer, J. A. de Gouw, A. Hansel, A. Jefferson, D.  
27 Kley, A. T. J. de Laat, S. Lal, M. G. Lawrence, J. M. Lobert, O. L. Mayol-Bracero, A. P. Mitra, T.  
28 Novakov, S. J. Oltmans, K. A. Prather, T. Reiner, H. Rodhe, H. A. Scheeren, D. Sikka, J.  
29 Williams, The Indian Ocean Experiment: Widespread air pollution from south and Southeast  
30 Asia, Science, 291, 1031–1036, 2001.

31 Liu, G., D. W. Tarasick, V. E. Fioletov, C. E. Sioris, and Y. J. Rochon, Ozone correlation lengths  
32 and measurement uncertainties from analysis of historical ozonesonde data in North America and  
33 Europe, J. Geophys. Res., 114, D04112, doi:10.1029/2008JD010576, 2009.

1 Liu, G., J. Liu, D. W. Tarasick, V. E. Fioletov, J. Jin, O. Moeini, X. Liu, and C. E. Sioris, A  
2 global tropospheric ozone climatology from trajectory-mapped ozone soundings, *Atmos. Chem.*  
3 *Phys.* 13, 10659–10675, doi:10.5194/acp-13-10659-2013, 2013.

4 Liu, H., D. J. Jacob, I. Bey, R. M. Yantosca, B. N. Duncan, and G. W. Sachse, Transport  
5 pathways for Asian combustion outflow over the Pacific: Interannual and seasonal variations, *J.*  
6 *Geophys. Res.*, 108(D20), 8786, doi:10.1029/2002JD003102, 2003.

7 Liu, J., D. W. Tarasick, V. E. Fioletov, C. McLinden, T. Zhao, S. Gong, C. Sioris, J. J. Jin, G.  
8 Liu, and O. Moeini, A global ozone climatology from ozone soundings via trajectory mapping: a  
9 stratospheric perspective, *Atmos. Chem. Phys. Discuss.*, 13, 16831–16883, 2013.

10 Liu, J., J. R. Drummond, D. B. A. Jones, Z. Cao, H. Bremer, J. Kar, J. Zou, F. Nichitui, and J. C.  
11 Gille, Large horizontal gradients in atmospheric CO at the synoptic scale as seen by spaceborne  
12 Measurements of Pollution in the Troposphere, *J. Geophys. Res.*, 111, D02306,  
13 doi:10.1029/2005JD006076, 2006.

14 Liu, J., J. R. Drummond, Qinbin Li, John C. Gille, Daniel C. Ziskin, Satellite mapping of CO  
15 emission from forest fires in Northwest America using MOPITT measurements, *Remote Sens.*  
16 *Environ.*, 95, 502–516, 2005

17 Logan, J. A., M. J. Prather, S.C. Wofsy, and M. B. McElroy, Tropospheric chemistry: A global  
18 perspective, *J. Geophys. Res.*, 86, 7210–7254, 1981.

19 Luo, M., C. P. Rinsland, C. D. Rodgers, J. A. Logan, H. Worden, S. Kulawik, A. Eldering, A.  
20 Goldman, M. W. Shephard, M. Gunson, and M. Lampel, Comparison of carbon monoxide  
21 measurements by TES and MOPITT: Influence of a priori data and instrument characteristics on  
22 nadir atmospheric species retrievals, *J. Geophys. Res.*, 112, D09303,  
23 doi:10.1029/2006JD007663, 2007.

24 Marenco, A., Thouret, V., Nedelec, P., Smit, H., Helten, M., Kley, D., Karcher, F., Simon, P.,  
25 Law, K., Pyle, J., Poschmann, G., Wrede, R. V., Hume, C., and Cook, T.: Measurements of  
26 ozone and water vapour by Airbus in-service aircraft: The MOZAIC airborne program, An  
27 overview, *J. Geophys. Res.*, 103, 25631–25642, 1998.

28 Mauzerall, D. L., D. J. Jacob, S.-M. Fan, J. D. Bradshaw, G. L. Gregory, G. W. Sachse, and D.  
29 R. Blake, Origin of tropospheric ozone at remote high northern latitudes in summer, *J. Geophys.*  
30 *Res.*, 101, 4175–4188, 1996.

31 Mauzerall, D. L., D. Narita, H. Akimoto, L. Horowitz, S. Walters, D. A. Hauglustaine, and G.  
32 Brasseur, Seasonal characteristics of tropospheric ozone production and mixing ratios over East  
33 Asia: A global three dimensional chemical transport and model analysis, *J. Geophys. Res.*, 105,  
34 17,895– 17,910, 2000.

1 [Mauzerall, D. L., J. A. Logan, D. J. Jacob, B. E. Anderson, D. R. Blake, J. D. Bradshaw, B.](#)  
2 [Heikes, G. W. Sachse, H. Singh, B. Talbot, Photochemistry in biomass burning plumes and](#)  
3 [implications for tropospheric ozone over the tropical South Atlantic, J. Geophys. Res., 103,](#)  
4 [8401–8423, 1998.](#)

5 McKee, D. J. (Ed.): Tropospheric Ozone: Human Health and Agricultural Impacts, Boca Raton,  
6 Fla.: Lewis Publishers, 39-208, 1993.

7 Nédélec P., Cammas J. P., Thouret V., Athier G., Cousin J. M., Legrand C., Abonne C., Lecoœur  
8 F., Cayez G. and Marizy C., An Improved Infra-Red Carbon Monoxide Analyser for Routine  
9 Measurements aboard Commercial Airbus Aircraft : Technical Validation and First Scientific  
10 Results of the MOZAIC III Program, Atmos. Chem. And Phys., Vol. 3, pp 1551-1564, 2003.

11 Nédélec P., Thouret V., Brioude J., Sauvage B., and Cammas J.-P., Sthol A. : Extreme CO  
12 concentrations in the upper troposphere over North-East Asia in June 2003 from the in-situ  
13 MOZAIC aircraft data. Geophysical Research Letters, 32, L14807, doi:10.1029/2005GL023141,  
14 2005.

15 Nédélec, P., R. Blot, D. Boulanger, G. Athier, J.-M. Cousin, B. Gautron, A. Petzold, A. Volz-  
16 Thomas and V. Thouret, Instrumentation on commercial aircraft for monitoring the atmospheric  
17 composition on a global scale: the IAGOS system, technical overview of ozone and carbon  
18 monoxide measurements, Tellus B, 67, 27791, <http://dx.doi.org/10.3402/tellusb.v67.27791>,  
19 2015.

20 [Novelli, P. C., L. P. Steele, and P. P. Tans, Mixing ratios of carbon monoxide in the troposphere.](#)  
21 [J. Geophys. Res., 97, 20,731-20,750, 1992.](#)

22 Novelli, P. C., K. A. Masarie, P. P. Tans, and P. M. Lang, Recent changes in atmospheric carbon  
23 monoxide, Science, 263, 1587-1590, 1994.

24 Novelli, P. C., K. A. Masarie, P. M. Lang, B. D. Hall, R. C. Myers, and J. W. Elkins, Reanalysis  
25 of tropospheric CO trends: Effects of the 1997–1998 wildfires, J. Geophys. Res., 108(D15),  
26 4464, doi:10.1029/2002JD003031, 2003.

27 Novelli, P. C., Masarie, K. A., Lang, P. M., Distributions and recent changes of carbon monoxide  
28 in the lower troposphere, J. Geophys. Res., 103 (D51), 19015–19033, 1998.

29 Osman, M., D. W. Tarasick, J. Liu, V. Thouret, V. E. Fioletov, O. Moeini, C. McLinden, C.  
30 Sioris, M. Parrington and P. Nédélec: Ozone climatology derived from the Trajectory Mapping  
31 of Global aircraft (MOZAIC-IAGOS), satellite (ACE-FTS, SAGE) and extended ozonesonde  
32 data, in preparation, [20152016](#).

33 Pan, L. L., Konopka, P., and Browell, E. V.: Observations and model simulations of mixing near  
34 the extratropical tropopause, J. Geophys. Res., 111(D05106), doi:10.1029/2005JD006480, 2006.

- 1 ~~Parrish, D. D., Carbon monoxide and light alkanes as tropospheric tracers of anthropogenic~~  
2 ~~ozone, The Tropospheric Chemistry of Ozone in the Polar Regions, edited by H. Niki and K.H.~~  
3 ~~Becker, 155-169, Springer-Verlag, Berlin, 1993.~~
- 4 ~~Parrish, D. D., J. S. Holloway, M. Trainer, P. C. Murphy, G. L. Forbes, and F. C. Fehsenfeld,~~  
5 ~~Export of North American ozone pollution to the North Atlantic Ocean, Science, 259, 1436-~~  
6 ~~1439, 1993.~~
- 7 Parrish, D. D., M. Trainer, J. S. Holloway, J. E. Yee, M. S. Warshawsky, F. C. Fehsenfeld, G. L.  
8 Forbes, and J. L. Moody, Relationships between ozone and carbon monoxide at surface sites in  
9 the North Atlantic region, J. Geophys. Res., 103, 13,357– 13,376, 1998.
- 10 Parrish, D. D., M. Trainer, M.P. Buhr, B. A. Watkins, and F. C. Fehsenfeld, Carbon monoxide  
11 concentrations and their relation to concentrations of total reactive oxidized nitrogen at two rural  
12 U.S. sites, J. Geophys. Res., 96, 9309-9320, 1991.
- 13 Petetin, H., Thouret, V., Fontaine, A., Sauvage, B., Athier, G., Blot, R., Boulanger, D., Cousin,  
14 J.-M., and Nédélec, P.: Characterizing tropospheric ozone and CO around Frankfurt between  
15 1994–2012 based on MOZAIC-IAGOS aircraft measurements, Atmos. Chem. Phys. Discuss.,  
16 15, 23841-23891, doi:10.5194/acpd-15-23841-2015, 2015.
- 17 Petzold, A., V. Thouret, C. Gerbig, A. Zahn, C.A.M. Brenninkmeijer, M. Gallagher, M.  
18 Hermann, M. Pontaud, H. Ziereis, D. Boulanger, J. Marshall, P. Nédélec, H.G.J. Smit, U. Frieß,  
19 J.-M. Flaud, A. Wahner, J.-P. Cammas, A. Volz-Thomas, and IAGOS Team., Global-scale  
20 atmosphere monitoring by in-service aircraft – current achievements and future prospects of the  
21 European research infrastructure IAGOS. Tellus B, 67,  
22 <http://dx.doi.org/10.3402/tellusb.v67.28452>, 2015.
- 23 Ploeger, F., Konopka, P., Günther, G., Groö, J.-U., and Müller, R.: Impact of the vertical  
24 velocity scheme on modeling transport across the tropical tropopause layer, J. Geophys. Res.,  
25 115, D03301, doi: 10.1029/2009JD012023, 2010.
- 26 Ploeger, F., Konopka, P., Müller, R., Günther, G., Groö, J.-U., Schiller, C., Ravegnani, F.,  
27 Ulanovski, A., and Riese, M.: Backtrajectory reconstruction of water vapour and ozone in-situ  
28 observations in the TTL, Meteorol. Z., 21(3), 239–244, 2012.
- 29 Pommrich, R., Müller, R., Groö, J.-U., Konopka, P., Ploeger, F., Vogel, B., Tao, M., Hoppe,  
30 C. M., Günther, G., Spelten, N., Hoffmann, L., Pumphrey, H.-C., Viciani, S., D’Amato, F.,  
31 Volk, C. M., Hoor, P., Schlager, H., and Riese, M.: Tropical troposphere to stratosphere transport  
32 of carbon monoxide and long-lived trace species in the Chemical Lagrangian Model of the  
33 Stratosphere (CLaMS), Geosci. Model Dev., 7, 2895–2916, doi:10.5194/gmd-7-2895-2014,  
34 2014.

- 1 Reichle, H. G., Jr., H. G. Reichle Jr., B. E. Anderson, V. S. Connors, T. C. Denkins, D. A.
- 2 Forbes, B. B. Gormsen, R. L. Langenfelds, D. O. Neil, S. R. Nolf, P. C. Novelli, N. S.
- 3 Pougatchev, M. M. Roell, L. P. Steele., Space shuttle based global CO measurements during
- 4 April and October 1994, MAPS instrument, data reduction, and data validation, J. Geophys.
- 5 Res., 104, 21,443–21,454, 1999.
- 6 Reichle, H. G., Jr., V. S. Connors, J. A. Holland, R. T. Sherrill, H. A. Wallio, J. C. Casas, E. P.
- 7 Condon, B. B. Gormsen, W. Seiler, The distribution of middle tropospheric carbon monoxide
- 8 during early October 1984, J. Geophys. Res., 95(D7), 9845-9856, 1990.
- 9 Rinsland, C .P., and J.S. Levine, Free tropospheric carbon monoxide concentrations in 1950 and
- 10 1951 deduced from infrared total column amount measurements, Nature, 318, 250-254, 1985.
- 11 Rinsland, C. P., Jones, N. B., Connor, B. J., Wood, S. W., Goldman, A., Stephen, T. M.,
- 12 Murcray, F. J., Chiou, L. S., Zander, R. & Mahieu, E., Multiyear infrared solar spectroscopic
- 13 measurements of HCN, CO, C<sub>2</sub>H<sub>6</sub>, and C<sub>2</sub>H<sub>2</sub> tropospheric columns above Lauder, New Zealand
- 14 (45 S Latitude). J. Geophys. Res., 107 (D14), 1-12, 2002.
- 15 Rodgers, C. D., Inverse Methods for Atmospheric Sounding: Theory and Practice, World Sci.,
- 16 Hackensack, N. J., 2000.
- 17 ~~Roelofs, G. J., and J. Lelieveld, Model study of the influence of cross tropopause O<sub>3</sub> transports~~
- 18 ~~on tropospheric O<sub>3</sub> levels, Tellus, 49B, 38–55, 1997.~~
- 19 -Sauvage B., V. Thouret, J.-P. Cammas, F. Gheusi, G. Athier, P. Nédélec, Tropospheric ozone
- 20 over Equatorial Africa : regional aspects from the MOZAIC data. Atmospheric Chemistry and
- 21 Physics, Vol. 5, pp 311-335, 2005.
- 22 Sauvage, B., F. Gheusi, V. Thouret, J.-P. Cammas, J. Duron, J. Escobar, C. Mari, P. Mascart, and
- 23 V. Pont, Medium-range mid-tropospheric transport of ozone and precursors over Africa: two
- 24 numerical case-studies in dry and wet seasons, Atmos. Chem. Phys., 7, 5357-5370, 2007.
- 25 Schoeberl, M. R., Douglass, A. R., Zhu, Z. X., and Pawson, S.: A comparison of the lower
- 26 stratospheric age spectra derived from a general circulation model and two data assimilation
- 27 systems, J. Geophys. Res., 108, 4113, DOI: 10.1029/2002JD002652, 2003.
- 28 Shindell, D.T., G. Faluvegi, D.S. Stevenson, M.C. Krol, L.K. Emmons, J.-F. Lamarque, G.
- 29 Pétron, F.J. Dentener, K. Ellingsen, M.G. Schultz, O. Wild, M. Amann, C.S. Atherton, D.J.
- 30 Bergmann, I. Bey, T. Butler, J. Cofala, W.J. Collins, R.G. Derwent, R.M. Doherty, J. Drevet,
- 31 H.J. Eskes, A.M. Fiore, M. Gauss, D.A. Hauglustaine, L.W. Horowitz, I.S.A. Isaksen, M.G.
- 32 Lawrence, V. Montanaro, J.-F. Müller, G. Pitari, M.J. Prather, J.A. Pyle, S. Rast, J.M.
- 33 Rodriguez, M.G. Sanderson, N.H. Savage, S.E. Strahan, K. Sudo, S. Szopa, N. Unger, T.P.C.
- 34 van Noije, and G. Zeng, Multi-model simulations of carbon monoxide: Comparison with

1 observations and projected near-future changes. *J. Geophys. Res.*, 111, D19306,  
2 doi:10.1029/2006JD007100, 2006.

3 Stein, O., M. G. Schultz, I. Bouarar, H. Clark, V. Huijnen, A. Gaudel, M. George, and C.  
4 Clerbaux, On the wintertime low bias of Northern Hemisphere carbon monoxide found in global  
5 model simulations, *Atmos. Chem. Phys.*, 14, 9295–9316, 2014.

6 Stohl, A. and Seibert, P., Accuracy of trajectories as determined from the conservation of  
7 meteorological tracers, *Q. J. R. Meteorol. Soc.*, 125: 1465–1484, 1998.

8 Stohl, A., Computation, accuracy and applications of trajectories - review and bibliography,  
9 *Atmos. Environ.* 32, 947-966, 1998.

10 Stohl, A., James, P., Forster, C., and Spichtinger, N.: An extension of Measurement of Ozone  
11 and Water Vapour by Airbus-In-service aircraft (MOZAIC) ozone climatologies using trajectory  
12 statistics, *J. Geophys. Res.*, 106, D21, 27,757-27,768, doi:10.1029/2001JD000749, 2001.

13 Tan, Q., Chameides, W. L., Streets, D., Wang, T., Xu, J., Bergin, M., and Woo, J.: An evaluation  
14 of TRACE-P emission inventories from China using a regional model and chemical  
15 measurements, *J. Geophys. Res.*, 109, D22305, doi:10.1029/2004JD005071, 2004.

16 Tarasick, D. W., Jin, J. J., Fioletov, V. E., Liu, G., Thompson, A. M., Oltmans, S. J., Liu, J.,  
17 Sioris, C. E., Liu, X., Cooper, O. R., Dann, T., and Thouret, V.: High-resolution tropospheric  
18 ozone fields for INTEX and ARCTAS from IONS ozonesondes, *J. Geophys. Res.*, 115, D20301,  
19 doi:10.1029/2009JD012918, 2010.

20 Thompson, A. M.: The oxidizing capacity of the Earth's atmosphere-Probable past and future  
21 changes, *Science*, 256, 1157–1165, doi:10.1126/science.256.5060.1157, 1992.

22 Tie, X., G. P. Brasseur, C. Zhao, C. Granier, S. Massie, Y. Qin, P. Wang, G. Wang, P. Yang, A.  
23 Richter, Chemical characterization of air pollution in eastern China and the eastern United  
24 States, *Atmos. Environ.*, 40, 2607–2625, 2006.

25 Vogel, B., Pan, L. L., Konopka, P., Günther, G., Müller, R., Hall, W., Campos, T., Pollack, I.,  
26 Weinheimer, A., Wei, J., Atlas, E. L., and Bowman, K. P.: Transport pathways and signatures of  
27 mixing in the extratropical tropopause region derived from Lagrangian model simulations, *J.*  
28 *Geophys. Res.*, 116, D05306, doi:10.1029/2010JD014876, 2011.

29 Volz-Thomas A., Berg M., Heil T., Houben N., Lerner A., Petrick W., Raak D., Pätz H. -W.,  
30 Measurements of total odd nitrogen (NO<sub>y</sub>) aboard MOZAIC in-service aircraft: instrument  
31 design, operation and performance, *Atmospheric Chemistry and Physics*, Vol. 5, pp 583-595,  
32 2005

33 ~~Voulgarakis, A., P.J. Telford, A.M. Aghedo, P. Braesicke, G. Faluvegi, N.L. Abraham, K.W.~~  
34 ~~Bowman, J.A. Pyle, and D.T. Shindell: Global multi year O<sub>3</sub>-CO correlation patterns from~~

models and TES satellite observations. *Atmos. Chem. Phys.*, 11, 5819–5838, doi:10.5194/acp-11-5819-2011, 2011.

Wang, T., K. S. Lam, L. Y. Chan, M. A. Carroll, A. S.Y. Lee, Trace gas measurements in coastal Hong Kong during the PEM-WEST (B), *J. Geophys. Res.* Vol. 102, 28,575–28,588, 1997.

Wang, T., M. A. Carroll, G. M. Alber, K. R. Owens, K. A. Duderstadt, and A. Markevitch, D. Parrish, J. Holloway, and F. C. Fehsenfeld, G. Forbes and J. Ogren, Ground-based measurements of NO<sub>x</sub> and total reactive oxidized Nitrogen (NO<sub>y</sub>) at Sable Island, Nova Scotia during the NARE 1993 Summer Intensive, *J. Geophys. Res.*, 101, 28,991–29,004, 1996.

Wang, Y. X., McElroy, M. B., Wang, T., and Palmer, P. I.: Asian emissions of CO and NO<sub>x</sub>: Constraints from aircraft and Chinese station data, *J. Geophys. Res.*, 109, D24304, doi:10.1029/2004JD005250, 2004.

[WHO, Air quality guidelines for Europe, 2nd ed. Copenhagen, World Health Organization Regional Office for Europe, 2000 \(WHO Regional Publications, European Series No. 91\), 2000](#)

[Worden, H. M., Deeter, M. N., Edwards, D. P., Gille, J. C., Drummond, J. R., and Nedelec, P.: Observations of near-surface carbon monoxide from space using MOPITT multispectral retrievals, \*J. Geophys. Res.\*, 115, D18314, doi:10.1029/2010JD014242, 2010.](#)

Worden, H. M., M. N. Deeter, C. Frankenberg, M. George, F. Nichitiu, J. Worden, I. Aben, K. W. Bowman, C. Clerbaux, P. F. Coheur, A. T. J. de Laat, R. Detweiler, J. R. Drummond, D. P. Edwards, J. C. Gille, D. Hurtmans, M. Luo, S. Martínez-Alonso, S. Massie, G. Pfister, and J. X. Warner,, Decadal record of satellite carbon monoxide observations, *Atmos. Chem. Phys.*, 13, 837–850, doi:10.5194/acp-13-837-2013, 2013.

Yurganov, L. N., McMillan, W., Dzhola, A. V., Grechko, E. I., Jones, N. B. & van der Werf, G. R., Global AIRS and MOPITT CO measurements: validation, comparison, and links to biomass burning variations and carbon cycle. *J. Geophys. Res.*, 113 (D9), 1–14, 2008).

~~Zahn, A., C. A. M. Brenninkmeijer, W. A. H. Asman, P. J. Crutzen, G. Heinrich, H. Fischer, J. W. M. Cuijpers, and P. F. J. van Velthoven, Budgets of O<sub>3</sub> and CO in the upper troposphere: CARIBIC passenger aircraft results 1997–2001, *J. Geophys. Res.*, 107(D17), 4337, doi:10.1029/2001JD001529, 2002.~~

Zander, R., P. Demoulin, D.H. Ehhalt, U. Schmidt, and C.P. Rinsland, Secular increase of the total vertical column abundance of carbon monoxide above central Europe since 1950, *J. Geophys. Res.*, 94, 11, 021–11,028, 1989.

[Zbinden, R. M., V. Thouret, P. Ricaud, F. Carminati, J.-P. Cammas, P. Nédélec, Climatology of pure tropospheric profiles and column contents of ozone and carbon monoxide using MOZAIC](#)



1 [in the mid-northern latitudes \(24° N to 50° N\) from 1994 to 2009, doi:10.5194/acp-13-12363-](#)  
2 [2013, 2013.](#)

3 Zeng, G., Wood, S. W., Morgenstern, O., Jones, N. B., Robinson, J. & Smale, D., Trends and  
4 variations in CO, C<sub>2</sub>H<sub>6</sub>, and HCN in the Southern Hemisphere point to the declining  
5 anthropogenic emissions of CO and C<sub>2</sub>H<sub>6</sub>, *Atmos. Chem. Phys.*, 12 (16), 7543-7555, 2012.

6 ~~Zhang, L., Jacob, D. J., Boersma, K. F., Jaffe, D. A., Olson, J. R., Bowman, K. W., Worden, J.~~  
7 ~~R., Thompson, A. M., Avery, M. A., Cohen, R. C., Dibb, J. E., Flock, F. M., Fuelberg, H. E.,~~  
8 ~~Huey, L. G., McMillan, W. W., Singh, H. B., and Weinheimer, A. J.: Transpacific transport of~~  
9 ~~ozone pollution and the effect of recent Asian emission increases on air quality in North~~  
10 ~~America: an integrated analysis using satellite, aircraft, ozonesonde, and surface observations,~~  
11 ~~*Atmos. Chem. Phys.*, 8, 6117–6136, doi:10.5194/acp-8-6117-2008, 2008.~~

12 Zhang, L., Jacob, D. J., Liu, X., Logan, J. A., Chance, K., Eldering, A., and Bojkov, B. R.:  
13 Intercomparison methods for satellite measurements of atmospheric composition: application to  
14 tropospheric ozone from TES and OMI, *Atmos. Chem. Phys.*, 10, 4725–4739, doi:10.5194/acp-  
15 10-4725-2010, 2010.

16